IEEE Access
Multidisciplinary ⋮ Rapid Review ⋮ Open Access Journal

Received 17 March 2026, accepted 1 April 2026, date of publication 9 April 2026, date of current version 24 April 2026.

Digital Object Identifier 10.1109/ACCESS.2026.3682547

RESEARCH ARTICLE

The Green Co-Driver: A Human-Interactive Self-Driving System That Improves the Energy Efficiency of Road Vehicles

MAURO DA LIO[1], (Member, IEEE), VISHNUVARDHAN SHAKTHIBALA[2], ANTONELLO CHERUBINI[3], GASTONE PIETRO ROSATI PAPINI[1], (Member, IEEE), STEFANO MELZI[4], (Member, IEEE), ALESSANDRO REGAZZETTI[4], STEFANO LOVATO[5], AND ROBERTO LOT[5]

[1]Department of Industrial Engineering, Università degli Studi di Trento, 38123 Trento, Italy
[2]Department of Electrical and Energy Engineering, Sapienza Università di Roma, 00138 Rome, Italy
[3]Department of Industrial Engineering, Alma Mater Studiorum—Università di Bologna, 40136 Bologna, Italy
[4]Department of Mechanical Engineering, Politecnico di Milano, 20156 Milan, Italy
[5]Department of Industrial Engineering, Università degli Studi di Padova, 35131 Padua, Italy

Corresponding author: Mauro Da Lio (mauro.dalio@unitn.it)

This work was supported by Italian Ministry of University and Research and European Union through NextGenerationEU, Mission 4 Component 2. Progetti di Rilevante Interesse Nazionale (PRIN) 2022 Prot. n. 2022W733FA, under Grant CUP E53D23003780006.

ABSTRACT This paper presents the design and experimental evaluation of a green driving function that balances energy efficiency and human driver expectations through a user-adjustable trade-off parameter. The function operates as a high-level advisory layer that provides eco-driving speed recommendations on top of an Advanced Driver Assistance System controlling longitudinal motion, making it portable across different advanced driver assistance and self-driving architectures. The system was tested in two different driving simulators with a total of 72 participants (aged 18-65), analyzing both quantitative performance metrics and subjective user evaluations. Quantitative metrics (e.g., energy consumption, travel time, and speed profiles) indicate that, in the considered simulator-based scenario and at the trade-off setting preferred by participants, increasing travel time by approximately 13.5% reduces energy consumption by about 34%, which corresponds to an increase in vehicle range of approximately 52% for the given vehicle characteristics. Additionally, the system exhibits negligible variability across repeated trials under identical simulated conditions, in contrast to the substantial variability observed in human coasting behavior, thereby eliminating human variations that negatively impact energy consumption. Subjective results show that, while manual driving is perceived as more fun, people are willing to adopt the system when confronted with a large extension of vehicle range at minimal travel time cost.

INDEX TERMS Advanced driver assistance systems, autonomous vehicles, driver behavior, driving simulators, electric vehicles, green transportation, intelligent vehicles, human–vehicle systems.

I. INTRODUCTION

A. STATE OF THE ART OF ECOLOGICAL DRIVING

Reducing energy consumption and emissions of road vehicles has become a major research focus in the last few decades. Two complementary directions have emerged: (a) the electrification of vehicle powertrains [1], and (b) the promotion of eco-driving by guiding drivers toward more environmentally friendly behaviors [2], [3].

Electrifying vehicles has become a key approach to lowering both energy use and emissions [4]. However, concerns about driving range—often referred to as range anxiety—reduce user acceptance and restrict market adoption. Consequently, enhancing energy efficiency—and thereby extending

The associate editor coordinating the review of this manuscript and approving it for publication was Jie Gao.

vehicle range—remains a key objective to make electric vehicles more attractive to consumers. Energy efficiency can be increased by optimizing powertrain components—such as the motor and energy storage systems [5]—or by advancing energy management strategies [6]. Over the last decade, various methods have been proposed to enhance powertrain efficiency, see e.g. [7] and [8]. These studies typically assume a predefined driving cycle and neglect the influence of driving behavior on energy consumption.

In this context, eco-driving has become a key strategy for reducing fuel or electrical energy consumption and emissions [9]. For conventional powertrains, research shows that adopting a more economical and environmentally conscious driving style can reduce fuel consumption by 5–10% [10], [11]. Moreover, eco-driving controllers have been introduced for hybrid [12] and electric vehicles [13], where the potential energy savings can exceed those achievable with conventional vehicles [14]. Eco-driving principles have been applied in a variety of driving scenarios, including car-following situations [15], cornering maneuvers [16], signalized intersections [17], [18], and roads with varying slopes [19]. The potential availability of vehicle connectivity has motivated the development of eco-driving speed advisory systems for connected vehicles [20], [21], [22], [23]. However, the limited penetration of vehicle-to-everything (V2X) technologies poses significant challenges for deploying eco-driving strategies in mixed traffic environments that include both connected and unconnected human-driven vehicles [24]. Optimal and model predictive control (MPC) formulations are especially relevant for autonomous vehicles, where eco-driving controllers can be applied directly to longitudinal control. They can also be embedded in driver assistance systems, such as speed advisory functions and adaptive cruise control [25].

Human-centered evaluations of eco-driving assistance systems have also been reported. In [26], an eco-driving advisory system is tested with human participants in a dynamic driving simulator. The system uses MPC to recommend energy-minimizing speeds from onboard sensor data, traffic light information, and route data. Simulator experiments showed energy savings of up to 10%, along with fewer speed limit violations and unnecessary stops at signalized intersections. A user questionnaire indicated that willingness to adopt the system depends strongly on perceived usefulness and confidence in its effective use. This prior work focuses on improving energy efficiency under safety constraints, whereas the present study explicitly balances user acceptance with ecological performance to foster adoption.

The review in [27] focuses on automating the driving task, with limited attention to user preferences. However, drivers exhibit diverse driving styles [28], and accounting for these differences is essential for system acceptance. To address this issue, a driver preference model for eco-driving in electric vehicles is proposed in [29] and [30] within an optimal control framework. It generates a reference speed profile from available vehicle and environmental information to minimize energy consumption while ensuring safety. The controller can be tuned to match driver preferences for speed, spacing, acceleration, and cornering speed.

Eco-driving can be integrated with self-driving functions that explicitly aim to align vehicle behavior with human intentions. For example, in the EU H2020 Dreams4Cars project (www.dreams4cars.eu), a self-driving agent able to comply with human wishes was developed and demonstrated emergent behaviors in [31]. Its architecture partly replicates human sensorimotor organization [32], implementing an artificial self-driving agent with a ''like human'' [33] decision-making system. This facilitates human–vehicle cooperation and, in this case, cooperation with the eco-driving recommendations.

Although eco-driving optimization, speed advisory systems, and autonomous or assisted driving architectures are well studied individually, their experimental validation in an integrated, human-interactive framework that explicitly balances energy efficiency and driver expectations remains limited.

B. PAPER CONTRIBUTION

This work addresses this limitation not by proposing a new eco-driving optimal-control formulation, but by presenting a system-level experimental proof of concept in which the trade-off between ecological performance and naturalistic driving behavior is explicitly modeled and can be tuned at runtime.

The proposed framework integrates established eco-driving optimal-control strategies with a naturalistic driver-preference model and a human-interactive co-driver architecture. Hence, the primary contribution lies in the system-level integration and behavioral validation of the efficiency–acceptance trade-off, rather than in isolated algorithmic novelty.

Energy-efficient driving, or eco-driving for short, requires, for example, gentle acceleration and the avoidance of braking by anticipating traffic situations. These behaviors demand substantial anticipation, which in turn increases the driver's workload and tends to increase travel time. As a result, drivers' acceptance of eco-driving is often poor. To increase user acceptance while maintaining driving efficiency, the Green Co-Driver is designed as a human-interactive driving system that:

a) prioritizes safety,
b) maximizes energy savings whenever this does not conflict with safety or user preferences,
c) adapts to human preferences, explicitly trading energy efficiency for user satisfaction in a controlled and acceptable way.

The Green Co-Driver has been implemented in two different driving simulator environments and tested with a total of 72 participants (aged 18–65). The results indicate that, while the Green Co-Driver operates at a slightly slower yet acceptable pace, it provides significant energy savings and

increased range. Furthermore, under the controlled simulator conditions, the Green Co-Driver exhibited more regular longitudinal behavior and reduced variability in energy consumption compared to human drivers.

The main contributions of this paper can be summarized as follows:

- system-level integration of eco-driving optimal control and a naturalistic driver-preference model within a human-interactive co-driver architecture,
- an adjustable eco-driving bias parameter (w) that explicitly trades energy efficiency against human driving expectations at runtime;
- an experimental evaluation with human participants in two driving simulators, assessing both objective energy-related metrics and subjective user acceptance.

The experimental evaluation is intended as a controlled, simulator-based proof of concept aimed at comparative and behavioral assessment, rather than as a substitute for on-road vehicle testing.

The remainder of the paper is organized as follows. Section II presents the Green Co-Driver assistant system and the underlying background. It first introduces a realistic model of an electric vehicle powertrain with driving losses (Section II-A) and a naturalistic virtual driver model. These vehicle and driver models are then integrated into an optimal control problem that generates a recommended speed profile that minimizes energy use while accommodating driver preferences for speed and acceleration (Section II-B). Examples of speed recommendations are provided, illustrating how energy is lost (Section II-C). The Green Co-Driver is subsequently incorporated into an automated driving function that prioritizes safety and necessary driving maneuvers, while yielding energy efficiency whenever possible (Section II-D).

Section III reports on the implementation of the Green Co-Driver system in two different driving simulators and its evaluation in two experimental campaigns with everyday drivers. The test protocols are detailed in Section III-A. Objective experimental results are analyzed in Section III-B, while subjective results are presented in Section III-C.

Finally, the discussion and conclusions are provided in Sections IV and V, respectively.

II. THE GREEN CO-DRIVER ASSISTANT SYSTEM

The conceptual system architecture is shown in Fig. 1. An automated driving function (ADF) — which may range from a simple Adaptive Cruise Control (ACC) to a full-fledged Level 4 self-driving system — controls the longitudinal dynamics of a vehicle.

The ADF is supported by the Green Driving Function (GDF), which operates as a high-level advisory layer and uses a subset of the ADF inputs together with electronic-horizon data to compute an optimized speed policy. This policy is provided in the form of an eco-driving directive, such as a recommended cruising speed (e.g., the requested speed input of an ACC).

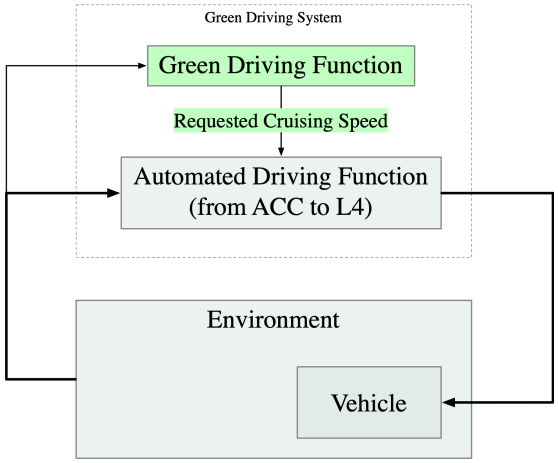

FIGURE 1. Conceptual system architecture. High-level architectural view of the Green Co-Driver, which provides eco-driving speed advice to an automated driving function; trajectory planning, motion control, and safety-critical decisions are handled by the underlying system, which may override the recommendation when required.

A fully self-contained autonomous driving system would need to address all aspects of the driving task, including safety monitoring. In contrast, the GDF is intentionally designed to focus on a single high-level role: the generation of eco-driving directives, while leaving execution and safety enforcement to the underlying driving system.

This separation improves modularity, supports scalability across different levels of automation, and allows the GDF to be ported across vehicle platforms without modifying safety-critical control layers.

Whenever possible, the ADF follows the eco-driving directive generated by the Green Driving Function. However, when required—for example, to avoid collisions or comply with temporary speed limits—the ADF may maneuver differently.

In this way, the GDF acts as an advisor that biases longitudinal behavior toward energy efficiency, whereas the ADF remains fully responsible for interpreting the directive in relation to the environment, enforcing safety constraints, and overriding the recommendation whenever safety or operational requirements dominate.

A. VEHICLE POWER LOSSES MODEL BACKGROUND

A front-wheel-drive electric vehicle (EV) is modeled by accounting for all significant power losses in both the vehicle and its powertrain, and including regenerative braking, which improves overall efficiency. The architecture of the system is shown in Fig. 2. It is adapted from [30], where more model details and numerical data can be found. Here, we summarise the aspects related to the evaluation of energy usage and its minimization. The different sources of losses in the vehicle may be classified as follows:

$$L_t = L_v + L_e + L_i, \tag{1}$$

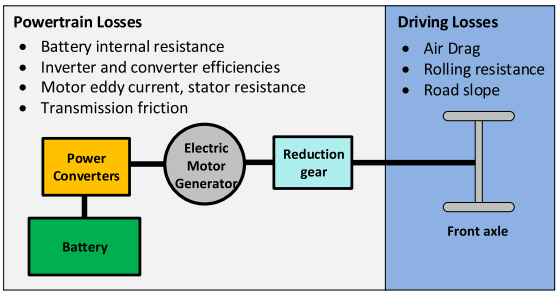

FIGURE 2. Electric vehicle powertrain architecture with power losses in evidence (from [30]).

TABLE 1. Vehicle main characteristics.

Symbol	Value	Description
m	1500 kg	vehicle mass
$\rho A C_d$	0.86 kg m^{-1}	coefficient of drag
c_{rr}	0.01	coefficient of rolling resistance
$q = \omega_e / v$	25.4 rad/m	motor-to-vehicle velocity ratio
β_r	0.5	regenerative braking bias
$P_{m,\max}$	80 kW	Motor peak power
$T_{m,\max}$	280 Nm	Motor maximum torque
$T_{r,\max}$	280 Nm	Generator maximum torque
$P_{r,\max}$	80 kW	Generator peak power

where L_t is the overall power loss, L_v the loss associated to the driving forces, L_e the losses in the powertrain, and L_i the idling losses.

1) DRIVING LOSSES

There are three main sources of vehicle driving losses:

- the tyre friction $F_t = c_{rr} mg \cos\theta$, where c_{rr} is the rolling resistance coefficient, mg the vehicle weight, and θ the road gradient.
- the air drag resistance $F_a = \frac{1}{2}\rho A C_d v^2$, where ρ is the air density, A the frontal area, C_d the drag coefficient, and v is the vehicle speed;
- the (non-negative) mechanical braking force F_f.

By adding up these three forces, the overall driving power loss reads:

$$L_v = \left(F_f + mgc_{rr} \cos\theta + \frac{1}{2}\rho C_d A v^2 \right) v. \tag{2}$$

2) POWERTRAIN LOSSES

As shown in Fig. 2, the powertrain comprises a battery pack that powers a synchronous electric motor via power converters (a DC-DC converter and a DC-AC inverter), with the motor then coupled to the front wheels via a fixed reduction gear. The powertrain is reversible, allowing regenerative braking, in which case the power flow is in the opposite direction to that during driving.

The main losses in the powertrain include: transmission friction losses, electric motor/generator losses due to stator resistance, eddy currents, bearing friction, and aerodynamic resistance, inverter and converter losses, and battery charge and discharge losses. Powertrain losses depend on the motor torque and speed, which in turn are proportional to the vehicle speed v and driving force at the wheel F_m via the fixed motor-to-vehicle velocity ratio q. In general terms, we may write:

$$L_e = L_e(v, F_m). \tag{3}$$

To obtain the explicit expression of losses $L_e(v, F_m)$, we start from the vehicle longitudinal dynamics, which is described by Newton's second law as:

$$m\dot{v} = F_m - \left(F_f + \frac{1}{2}\rho A C_d v^2 + c_{rr} mg \cos\theta \right) - mg \sin\theta. \tag{4}$$

The driving force may be isolated as:

$$F_m = \left(F_f + \frac{1}{2}\rho A C_d v^2 + c_{rr} mg \cos\theta \right) + m(\dot{v} + g \sin\theta), \tag{5}$$

where the first brackets enclose the dissipative forces, while the second ones encase the conservative forces (associated with the kinetic and potential energy, respectively). During deceleration or on a downhill slope, the conservative forces are negative and, if they exceed the dissipative forces, the electric power unit can be used as a generator to recover energy. However, the generator alone cannot guarantee full braking performance because its peak torque $T_{r,\max}$ and maximum power $P_{r,\max}$ are insufficient for important decelerations or high speeds. Additionally, the electrical braking system operates only on the front axle, raising safety concerns about potential instability during severe decelerations. Therefore, electric braking is supplemented by hydraulic brakes on both the front and rear axles and cannot completely recover energy. By isolating from Equation (5) the overall longitudinal force required at the wheel:

$$F = \frac{1}{2}\rho A C_d v^2 + c_{rr} mg \cos\theta + m(\dot{v} + g \sin\theta), \tag{6}$$

the driving force associated with the power units, under both driving and braking conditions, reads:

$$F_m = \begin{cases} F, & F \geq 0, \\ -\min\left(\beta_r |F|,\ qT_{r,\max},\ \dfrac{P_{r,\max}}{v} \right), & F < 0. \end{cases} \tag{7}$$

where the *braking bias* β_r is the ratio between the front and total braking force. We can now calculate the powertrain losses [30], which are reported in Fig. 3 and, for computational efficiency, are approximated by a polynomial as follows:

$$L_e = a_{01} v + a_{11} F_m v + a_{20} F_m^2 + a_{30} F_m^3 + a_{21} F_m^2 v, \tag{8}$$

where the coefficients a_k have been determined with a least-squares fit.

3) IDLING LOSSES

For the sake of simplicity, the power necessary to run the on-board systems is assumed to be constant $L_i = 500$ W.

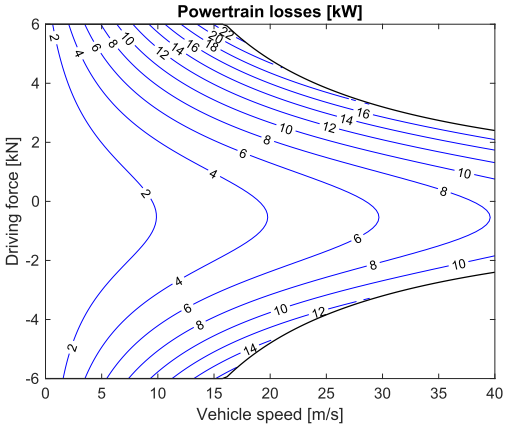

FIGURE 3. Approximated powertrain losses as a function of vehicle speed and electrical traction force. Note the asymmetry, caused by the battery power and current values being larger in magnitude under traction than braking.

B. THE GREEN DRIVING FUNCTION BACKGROUND

In this section, we describe the system architecture and summarize operating principles of the Green Co-Driver, which have been adapted from previous works [29], [30]. The goal of the Green Driving Function (GDF) is to determine a vehicle speed profile that minimizes energy consumption while accounting for the driver's preferences. From a mathematical perspective, the speed advisory problem is formulated within the framework of optimal control theory [34]:

$$\min_{\mathbf{u}\in\mathcal{U}} \quad J = \int_0^T L(\mathbf{x},\mathbf{u},t)\,dt, \tag{9a}$$

$$\text{s.t.} \quad \dot{\mathbf{x}} = \mathbf{f}(\mathbf{x},\mathbf{u}), \tag{9b}$$

$$\mathbf{g}(\mathbf{x},\mathbf{u}) \le \mathbf{0}, \quad \text{for all } t, \tag{9c}$$

$$\mathbf{b}(\mathbf{x}(0),\mathbf{x}(T)) = \mathbf{0}. \tag{9d}$$

where $J(\cdot)$ is the cost function to be minimized, (9b) describes the system dynamics, (9c) are inequality constraints, and (9d) represents the boundary conditions (where the travel time T is not pre-defined).

1) STATES, INPUTS, AND DYNAMICS

In the proposed formulation, the states are the longitudinal position along the route s and vehicle speed v:

$$\mathbf{x} = [s, v]^T. \tag{10}$$

There is only one control input, which is the overall longitudinal force F that is generated by the electric powertrain and, under braking, by the mechanical brakes:

$$\mathbf{u} = [F]. \tag{11}$$

The system dynamics are given by the longitudinal vehicle model described in the previous section, plus an integrator for determining the traveled space:

$$\dot{v} = \frac{F - \frac{1}{2}\rho A C_d v^2 - c_{rr} mg\cos\theta}{m} - g\sin\theta, \tag{9b.1}$$

$$\dot{s} = v. \tag{9b.2}$$

2) CONTRAINTS

The optimal control problem is subject to multiple constraints arising from vehicle limitations, environmental conditions, and driver preferences.

Vehicle constraints include motor torque and power limits as indicated in Table 1:

$$F - q\,T_{m,\max} \le 0, \tag{9c.1}$$

$$Fv - P_{m,\max} \le 0. \tag{9c.2}$$

The legal speed limit v_{sl} is enforces as follows:

$$v - v_{sl} \le 0. \tag{9c.3}$$

Driver's preferences include a cornering speed limit, which is calculated according to the modified Levison's fitting formula [35, Equation 7]:

$$v \le L_G\, v_0 \sqrt[4]{\sqrt{\frac{a_0^2}{\kappa^2 v_0^4} + \frac{1}{4}} - \frac{1}{2}}, \tag{9c.4}$$

where κ is the path curvature and $L_G = 1$, $v_0 = 14.84$ m/s, and $a_0 = 4.20$ m/s^2 are constants that describe the median driver.[1] In particular, L_G is used here as a convenient way to describe how faster or slower the observed behaviors are.

Additionally, the co-driver deceleration behavior mimics the human one, as shown in [37, Figure 8], with maximum deceleration of about 2 m/s^2 for the median driver. This limit cannot be enforced as a hard constraint, since emergencies may require substantially higher deceleration levels. Therefore, it is incorporated into the driver model as a *soft* constraint through a penalty function that increases rapidly when the limit is exceeded, see [30] for further details.

3) BOUNDARY CONDITIONS

In this problem, the vehicle starts with an initial speed $v_0 = 10$ m/s, the trip length $L = 10200$ m, while the traveling time T is free. Boundary conditions read:

$$s(0) = 0, \quad v(0) = v_0, \tag{9d.1}$$

$$s(T) = L, \quad v(T) = 0. \tag{9d.2}$$

4) COST FUNCTION AND TRADE-OFF BETWEEN ENERGY AND DRIVER PREFERENCES

The core of the Green Driving Function lies in the cost function (9a), which is defined as:

$$J = \int_0^T \left[(1-w)L_d + w\frac{L_t}{L_0}\right] dt. \tag{12}$$

[1] Given v and κ, the lateral acceleration in curves is determined, and follows naturalistic driving models [35], [36].

where L_d is a dimensionless function that embeds the driver's preferences, L_t are the vehicle power losses defined in (1), L_0 is a scale factor, and $w \in [0, 1]$ is the *eco-driving bias* that blends the two terms.

When the eco-driving bias is unitary ($w = 100\%$), the GDF cost function reduces to the (scaled) energy usage for the whole trip

$$J = \int_0^T \frac{L_t}{L_0}\, dt = \int_0^T \frac{L_v + L_e + L_i}{L_0}\, dt, \qquad (13)$$

where possible variations of kinetic and potential energy are not accounted for because speed and position are fixed both at the beginning and end of the trip. If we do not account for driving constraints (such as legal speed limits or the need to decelerate in a curve), the optimal control problem reduces to a simple constant-speed profile. In other words, the dynamic optimal control problem degenerates into a static minimization, whose objective is to determine the most efficient cruising speed. In our specific case, the most efficient speed is approximately 30 km/h, which is clearly not acceptable by drivers – and it is even dangerous on the highway.

When the eco-driving bias is null ($w = 0\%$), the GDF cost function reduces to the driver cost function $J_d = \int_0^T L_d dt$ that has been presented first in [29] and revised in [30]. These papers present a naturalistic driver model that accounts for driver preferences regarding acceleration, braking, following distance, and cornering. The speed prediction is based on minimizing J_d subject to constraints on longitudinal and lateral acceleration, thereby generating naturalistic speed profiles. The model can be tuned with a small set of physically meaningful parameters, and predicted speeds in car-following and cornering situations are compatible with real-world driving data [38]. All driver-model parameters used in this study correspond to those reported in [30], without additional tuning for the present experiments.

5) NUMERICAL SOLUTION AND IMPLEMENTATION

The problem is inherently non-convex due to the nature of the powertrain and braking losses and constraints. As we retain this non-convexity, there is no guarantee that a solution found by a direct method to solve the OCP is a global minimum. Nonetheless, we find that implementations of (9) perform well in practice.

When performing collocation and mesh refinement using an hp-adaptive solver (GPOPS-II [39] in our examples) with the interior point NLP solver IPOPT used to solve the resulting optimisation problems, the 10 km scenario considered here takes approximately 10 minutes of driving time and was solved in approximately 1 minute on a standard desktop PC equipped with an Intel i7 processor, corresponding to solution approximately 10 times faster than real time.

In the experimental validation presented in this paper, the optimal control problem was solved offline to generate reference speed profiles for the considered route. Given the layered architecture of Fig. 1, the Green Driving Function operates as a high-level advisory layer. It therefore does not require high-frequency receding-horizon updates, since the underlying automated driving function retains full authority to interpret or override the recommended speed in real time.

For completeness, we also explored the feasibility of faster receding-horizon updates by approximating the optimal policy with a neural-network surrogate. This verification did not modify the resulting speed recommendations and did not affect the experimental results reported in this study.

TABLE 2. Average speed and specific energy usage for different *eco-driving biases*.

case w	speed (km/h)	total (W/km)	tires (W/km)	powertrain (W/km)	drag (W/km)	braking (W/km)
0%	70.8	182.8	40.9	27.2	83.9	30.8
10%	61.2	120.5	40.9	20.2	47.2	12.3
50%	53.3	94.6	40.9	18.8	31.1	3.8

C. HOW THE ENERGY IS LOST

When the eco-driving bias is set to a value between 0 and 1, the GDF cost function combines energy savings with driving preferences, balancing energy losses against average speed. This is illustrated in Fig. 4, which shows the co-driver speed profiles for the test route depicted in Fig. 6. The profiles were calculated using three trade-offs between energy savings and travel time, specifically for $w = 0\%$, 10%, and 50%.

The highest average speed is achieved when $w = 0$, which represents naturalistic driving behavior. At the beginning of each highway segment, the vehicle accelerates to the legal speed limit of 130 km/h, then maintains that speed until it prepares to exit, at which point it begins to brake. A similar driving pattern is observed in the other rural sectors with 70 km/h and 90 km/h speed limits, although in the shortest segments, the speed limit may not be reached.

When the eco-driving bias is increased to $w = 10\%$ and $w = 50\%$, the speed limits are no longer reached because the GDF chooses lower accelerations and lower top speeds. Additionally, before highway exits, roundabouts, and curves, coasting down (which recovers kinetic energy) is preferred over braking (which dissipates energy). Curves are driven at the same speed regardless of w, as they mimic human speed choice (9c.4), and the safety and comfort requirements are the same.

The statistics for the different speed profiles are summarized in table 2. When the parameter w increases from 0% to 10%, the average speed decreases by approximately 14%, while energy usage decreases by 34%, corresponding to an increase of 52% in the vehicle's autonomy. Increasing w from 10% to 50% decreases the average speed by an additional 13%. The extra energy savings are only 22%, and the increase in autonomy is 27%.

The table also reports the specific energy losses per category: tire friction, powertrain, drag resistance, and

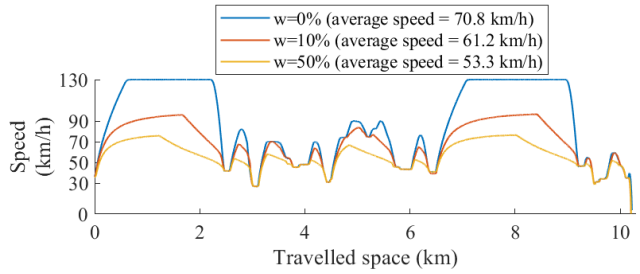

FIGURE 4. Speed profiles generated by the Green Driving Functions for different *eco-driving biases*.

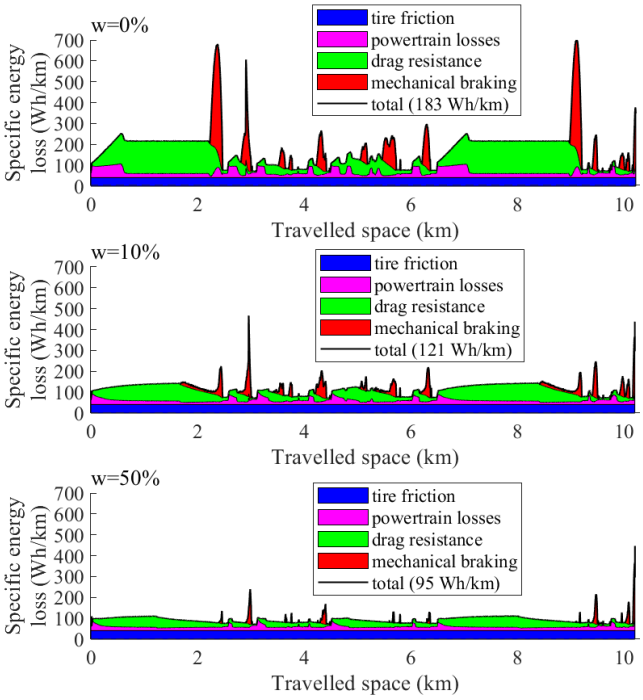

FIGURE 5. Specific energy losses per category (tire friction, powertrain, drag resistance, and mechanical braking losses) with three different eco-driving biases ($w = 0\%$, 10%, and 50%).

mechanical braking losses. The same categories are illustrated in Fig. 5, which shows where the losses occur along the route. Note that the specific energy usage is equivalent to the power loss divided by the speed, which has the dimension of a force. Therefore, tire-specific losses are simply proportional to the tire rolling resistance, which is independent of the speed and equal in all cases. Drag-specific losses are proportional to the square of the speed, so they decrease as w increases. Powertrain losses increase with the power demand; again, they diminish as w increases. Finally, mechanical braking losses are concentrated in the curve-entering sections; they are very high for $w = 0$ because the speed before cornering is high and coasting is not used.

D. THE AUTOMATED DRIVING FUNCTION (ADF)

In this paper, the automated driving function (ADF) shown in Fig. 1 corresponds to the self-driving system developed in a previous EU project [40] and described in detail in [41]. The system is capable of fully autonomous driving and exhibits emergent behaviors [42]. It can also collaborate with a human driver, whereby the driver's steering and pedal actions influence the system's decisions [31]; hence, it is also referred to as a "co-driver." To simplify interpretation of the driving simulator experiments, this dynamic interaction was disabled, and we instead evaluated four predefined speed–efficiency trade-offs, as described in Section III-A.

Regarding the integration with the green driving function (Fig. 1), the system interprets the eco-driving speed advice provided by the GDF within the context of the perceived environment and safety constraints, and it retains full authority to override the recommended speed to ensure safe operation [41, Section II-D-1].

III. SIMULATOR PILOT TESTS

Driving simulators are used to ensure repeatable experimental conditions, controlled exposure to different eco-driving strategies, and safe evaluation of user perception and acceptance, which would be difficult to isolate in real traffic.

Two different driving simulators were used: the semi-static, 3-degree-of-freedom (3 DOF) simulator at the University of Trento (UNITN) and the high-fidelity DIM 400 simulator at Politecnico di Milano (POLIMI). Additional details are available in the appendix. The two simulators differ in motion cueing, latency, and longitudinal control implementation, reflecting distinct levels of fidelity and actuation characteristics. Rather than seeking direct quantitative equivalence between platforms, the experiments were designed to assess whether behavioral trends and user evaluations remain consistent across different simulator configurations.

A. TEST PROTOCOLS

The simulators have been employed in experimental campaigns involving everyday drivers. The goals of the tests included:

- evaluating users' acceptance of green automated driving;
- understanding how to balance green versus naturalistic driving to boost acceptance;
- increasing awareness of eco-driving benefits;
- comparing results from the two simulators to assess if their features caused any difference.

Volunteers aged 18 to 65 were selected for the study. For the POLIMI simulator tests, 30 volunteers were recruited, evenly split by gender and age bin. In contrast, 44 individuals were initially recruited at UNITN; two discontinued due to simulator-induced motion sickness, and 42 completed the tests. The UNITN cohort was unbalanced across age and gender groups, with a majority of male participants. Only completed trials (total n = 72) are included in the analysis.

To execute the tests, a virtual scenario representative of a possible home-to-work commute was implemented in

the simulators. The virtual route is illustrated in Fig. 6; it extends approximately 11 km and includes two motorway sections, extra-urban sections, and a crossing of an urban center.

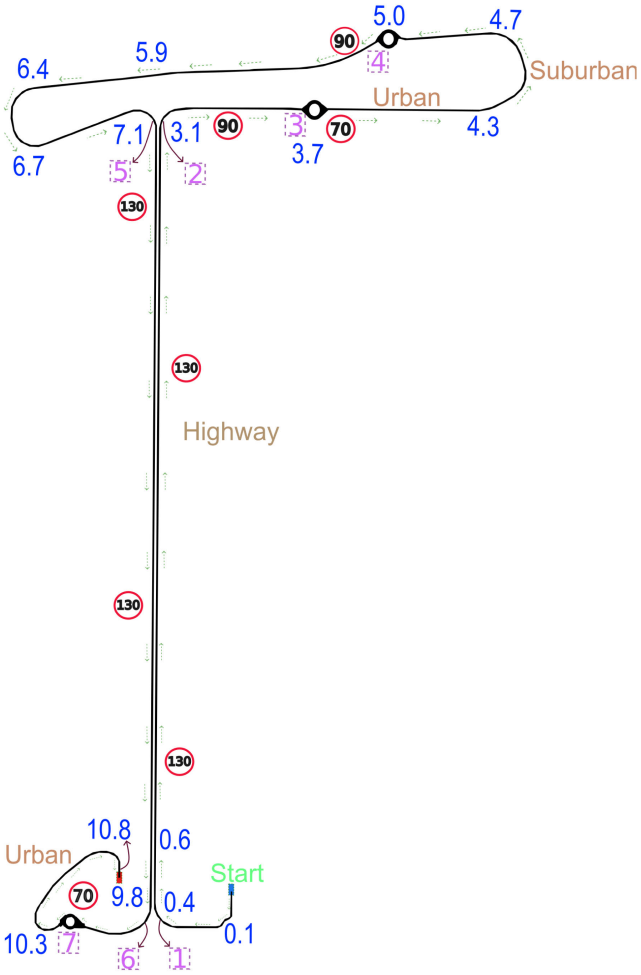

FIGURE 6. The test route features motorway, urban, and suburban sections with posted speed limits. The total distance from start, in kilometers, is indicated, and important landmarks are labeled.

The test protocol limited volunteers' time in the simulator to 45 minutes to prevent fatigue or discomfort. Each volunteer participated in four trials within a single session. In the first three trials, they acted as passengers in an autonomous vehicle, experiencing three levels of green-driving versus naturalistic-driving balance (0%, 10%, and 50%); the order of these trials was randomized for each participant. In the final trial, volunteers drove the route manually using their own driving style. After each trial, they rated various aspects of the experience on a scale from 1 to 6. More details are provided in Section III-C3. Participants were also asked about their intention to use the green-driving function if it were available on a real vehicle. During the manual-driving trial, travel time and energy consumption were also recorded (Section III-B).

1) ETHICAL APPROVALS

The experiments involving human participants conducted with the UNITN simulator were approved on December 18, 2024, by the University of Trento's Ethical Committee.

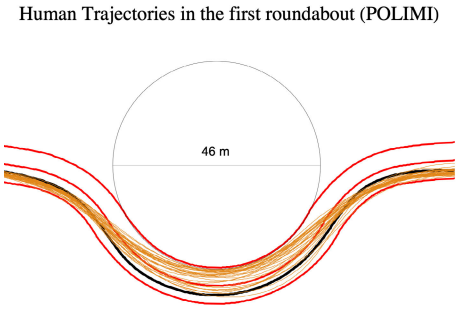

FIGURE 7. At roundabouts, if there are no obstacles, human drivers tend to take trajectories that cross the lane (orange lines). These paths can be faster than the co-driver, which consistently stays within its lane (represented by the black line). The picture refers to location 3.

The experiments involving human participants conducted with the POLIMI simulator were approved on May 5, 2023, by the Ethical Committee of Politecnico di Milano.

B. QUANTITATIVE TEST RESULTS

Our experiment was conducted with light traffic: the drivers or the co-driver were not penalized by obstacles because they were always able to overtake. This demonstrates the potential of a green driving policy in ideal conditions. Conversely, in congested traffic, the human driver's or co-driver's ability to choose an optimal speed is severely restricted, forcing them to follow the traffic flow without significant ability to enforce energy-saving behaviors.

1) DRIVER CLUSTERS BY SPEED CHOICE IN CURVES

In section II-C, we noted that the cornering speed chosen by the GDF depends on the road curvature and is independent of the green driving bias.

Conversely, substantial variations in cornering speed were observed among human drivers in the simulator experiments.

There is a substantial body of literature on how humans choose speed in curves, with a comprehensive summary provided in [35] and [36]. Notably, (9c.4) represents a modified version of Levison's formula, which aligns well with the median human driver, corresponding to $L_G = 1$. The gain L_G in (9c.4) can therefore be used to describe variations among drivers, indicating how fast a particular driver is relative to the median driver. In this formulation, the route curvature determines the cornering speed: the higher the curvature, the lower the speed.

Speed in curves is crucial for energy efficiency: the lower the speed, the more the vehicle must decelerate and then accelerate again, leading to greater energy losses, primarily through mechanical braking. Therefore, it is reasonable to expect that drivers who are faster than the median driver in

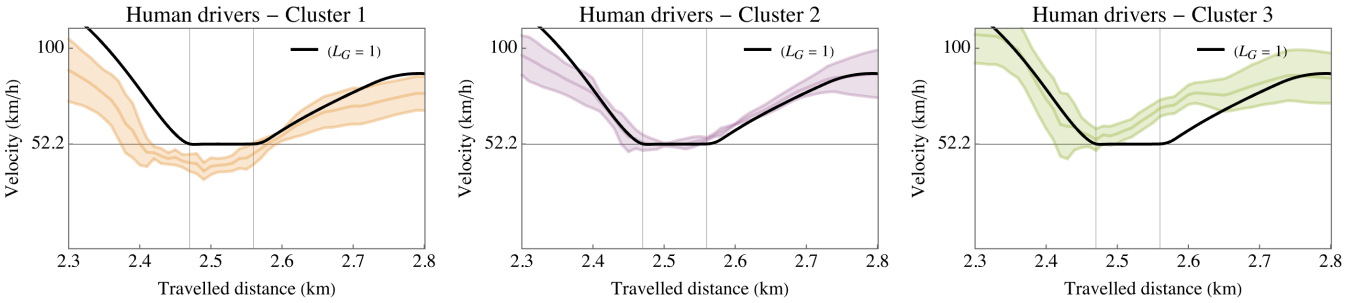

FIGURE 8. Speed of human drivers in the first exit ramp (location 2). The black line represents the median driver ($L_G = 1$). The colored lines represent the median speed profile across participants and the interquartile range (25th–75th percentile, shown as the shaded band). Left: participants slower than the median driver (Cluster 1: $L_G \leq 0.95$). Center: participants similar to the median driver (Cluster 2: $0.95 < L_G < 1.05$). Right: participants faster than the median driver (Cluster 3: $L_G \geq 1.05$).

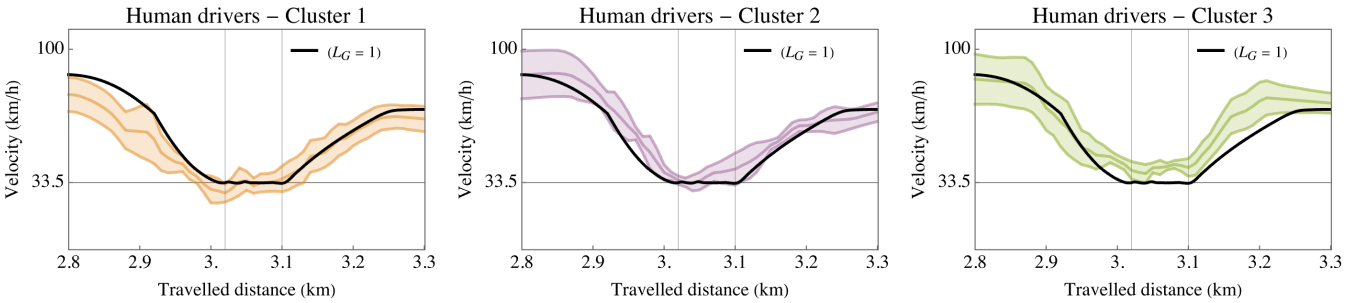

FIGURE 9. Speed of human drivers in the first roundabout (location 3). The same clusters as in Fig. 8 are shown. In multi-lane roundabouts, drivers tend to change lanes and straighten their path, achieving higher speeds than in single-lane curves.

curves ($L_G > 1$) will conserve more energy, as they rely less on regeneration and mechanical braking during deceleration and require less energy from the battery to resume their cruising speed.

To account for inter-driver variability in cornering behavior and its impact on energy efficiency, participants were clustered according to their curve-speed choice.

For clustering, the first exit ramp (Fig. 6, location 2) was selected as a representative case of a single-lane, isolated curve with well-defined curvature and distinct deceleration–cornering–acceleration phases. The mean curve speed in this segment was computed for each participant and used to estimate the corresponding effective gain parameter L_G relative to the median-driver reference ($L_G = 1$).

The clustering criterion was defined relative to the median-driver reference ($L_G = 1$): participants whose mean curve speed was within $\pm 5\%$ of the reference were assigned to Cluster 2 (median-like drivers), those more than 5% slower to Cluster 1, and those more than 5% faster to Cluster 3. The $\pm 5\%$ tolerance band was selected as a symmetric threshold around the median reference to distinguish clearly different cornering behaviors while maintaining a sufficient sample size within each group.

Figure 8 shows the speed profiles in the exit ramp (Fig. 6, location 2) for the three driver groups in the POLIMI experiment. The black line ($L_G = 1$) represents the median driver and corresponds to a curve speed of 52.5 km/h.

1) Cluster 1 consists of 13 participants who drove slower than the median driver ($0.62 \leq L_G < 0.95$).
2) Cluster 2 consists of 6 participants who drove similarly to the median driver.
3) Cluster 3 consists of 11 participants who drove faster than the median driver ($1.05 < L_G \leq 1.3$).

These clusters correspond to distinct longitudinal behaviors, with slower drivers exhibiting earlier and stronger braking before curves, median drivers showing more precise speed modulation with less variability, and faster drivers exhibiting earlier speed recovery. The vertical grid lines mark the beginning and end of the curve.

The first roundabout (location 3 in Fig. 6) is reported as a complementary case illustrating driver behavior in a multi-lane circular intersection. Fig. 7 shows that drivers tend to straighten their paths within the two-lane roundabout, effectively reducing the local curvature compared to a lane-constrained trajectory.

Figure 9 shows the speed profiles of the same clusters at the first roundabout. In this case, a median driver remaining in its lane would travel at 33.5 km/h. All clusters are shifted upward relative to the lane-constrained median-driver reference because drivers reduce the effective curvature by straightening their trajectory within the multi-lane roundabout, thereby achieving higher admissible speeds than the model that remains within a single lane.

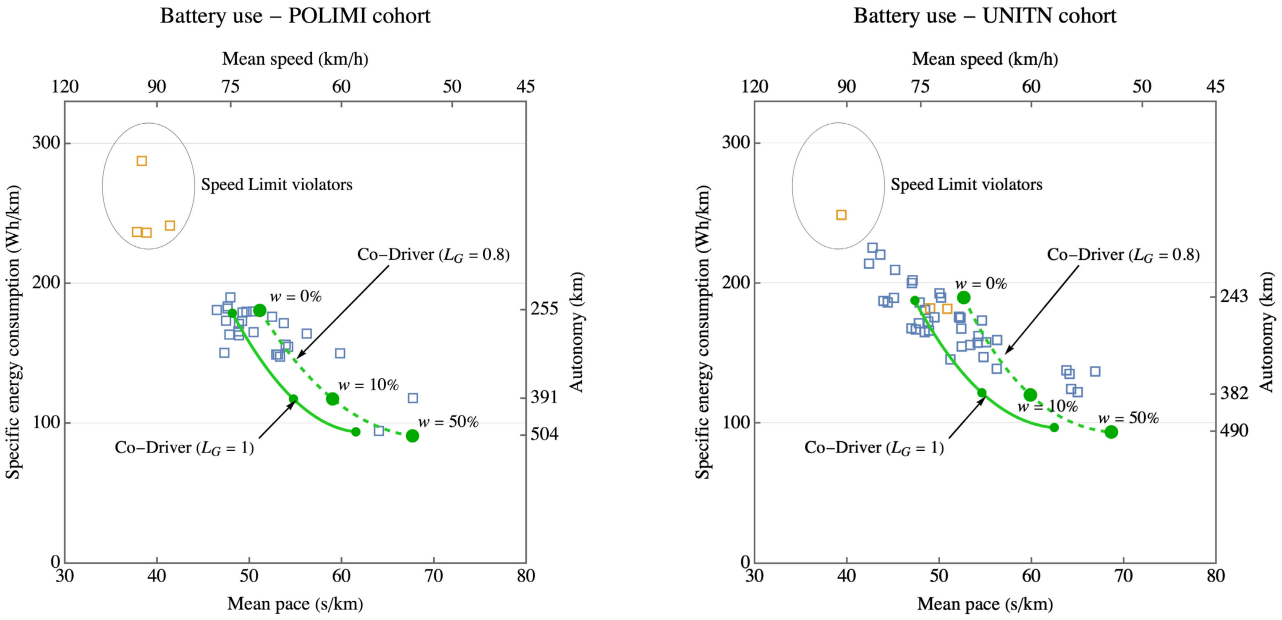

FIGURE 10. Comparison of specific energy consumption and average speed for the POLIMI (left) and UNITN (right) test participants. Squares indicate individual performance, with orange highlighting severe speed-limit violations. The green curves show two settings of the co-driver gain L_G, used for different purposes. The solid line, $L_G = 1$, corresponds to the median driver and serves as a baseline for efficiency analysis. The dashed line, $L_G = 0.8$, together with the three dots, shows the actual settings experienced by the participants in the simulators, where a lower L_G was used to reduce motion-sickness effects (only the subjective scores are affected by this setting). The longitudinal controller of the UNITN simulator, which takes the requested acceleration from the automated function in Fig. 1, was less precise and produced jerkier responses than the POLIMI controller. This led to less accurate execution and reduced efficiency, especially along the autonomy axis. These issues are more pronounced for the $L_G = 0.8$ and $w = 0$ conditions, which generate the highest decelerations.

2) ENERGY EFFICIENCY VERSUS TRAVEL TIME

Figure 10 illustrates the specific energy consumption (Wh/km) for the POLIMI and UNITN cohorts.

The solid green curve corresponds to the Green Co-Driver parametrized with $L_G = 1$, that is, using the same curve-speed choice as the median human driver. This curve represents the co-driver pace–consumption locus as the naturalistic–eco-driving bias w varies between 0% (top-left end) and 50%.

Most participants generally fell close to the upper end of this curve (near $w = 0\%$). Retrospectively, this suggests that the Green Co-Driver mimics the behavior of naturalistic drivers when it adopts the same longitudinal control criterion ($w = 0\%$) and curve-speed choice ($L_G = 1$).

Some participants appeared slightly to the left of the curve, indicating that they were somewhat faster than the Green Co-Driver at a similar level of energy consumption, potentially due to higher speeds when straightening their trajectories through the roundabouts. However, many were positioned to the right of the curve, including a long tail of slow drivers, suggesting that they were less efficient overall.

The participants highlighted in orange significantly exceeded the speed limit in both the motorway and suburban sections. We determined that they did not accurately perceive their speed in the driving simulator environment, which led to extremely high energy consumption.

The chart also shows a second green dashed curve, representing a co-driver parametrization with a slower speed choice in curves ($L_G = 0.8$), which will be explained in Section III-C.

The longitudinal controller of the UNITN simulator, which receives the requested acceleration from the automated system in Fig. 1, was less accurate and generated jerkier responses than the POLIMI controller. This resulted in less precise execution and reduced efficiency, as evidenced by the autonomy axes in Fig. 10. These issues are more pronounced for $w = 0$, which requires the highest decelerations. While these platform-specific characteristics affect the absolute execution accuracy, the relative trends observed across driving conditions remain consistent between the two simulators.

Figure 11 presents the test results for the three clusters separately. The participants in Cluster 1, who drove slower than the median driver, are generally positioned to the right of the co-driver with $L_G = 1$, with one marginal exception. They exhibit substantial variability in their distance from the Green Co-Driver curve, reinforcing the longitudinal control variability already noted in Figs. 8 and 9. The point associated with driver 30 of the POLIMI cohort is among the poorest performers. Figure 12 shows that this driver experienced a significant speed undershoot in both curves, which contributes to his reduced efficiency. These errors are likely due to an inaccurate perception of deceleration in the simulator and may not be as pronounced in real vehicles. The participants in Cluster 2, who are closer to the median driver, show less variation and align more closely with the co-driver $L_G = 1$ curve (Fig. 11). This outcome is consistent

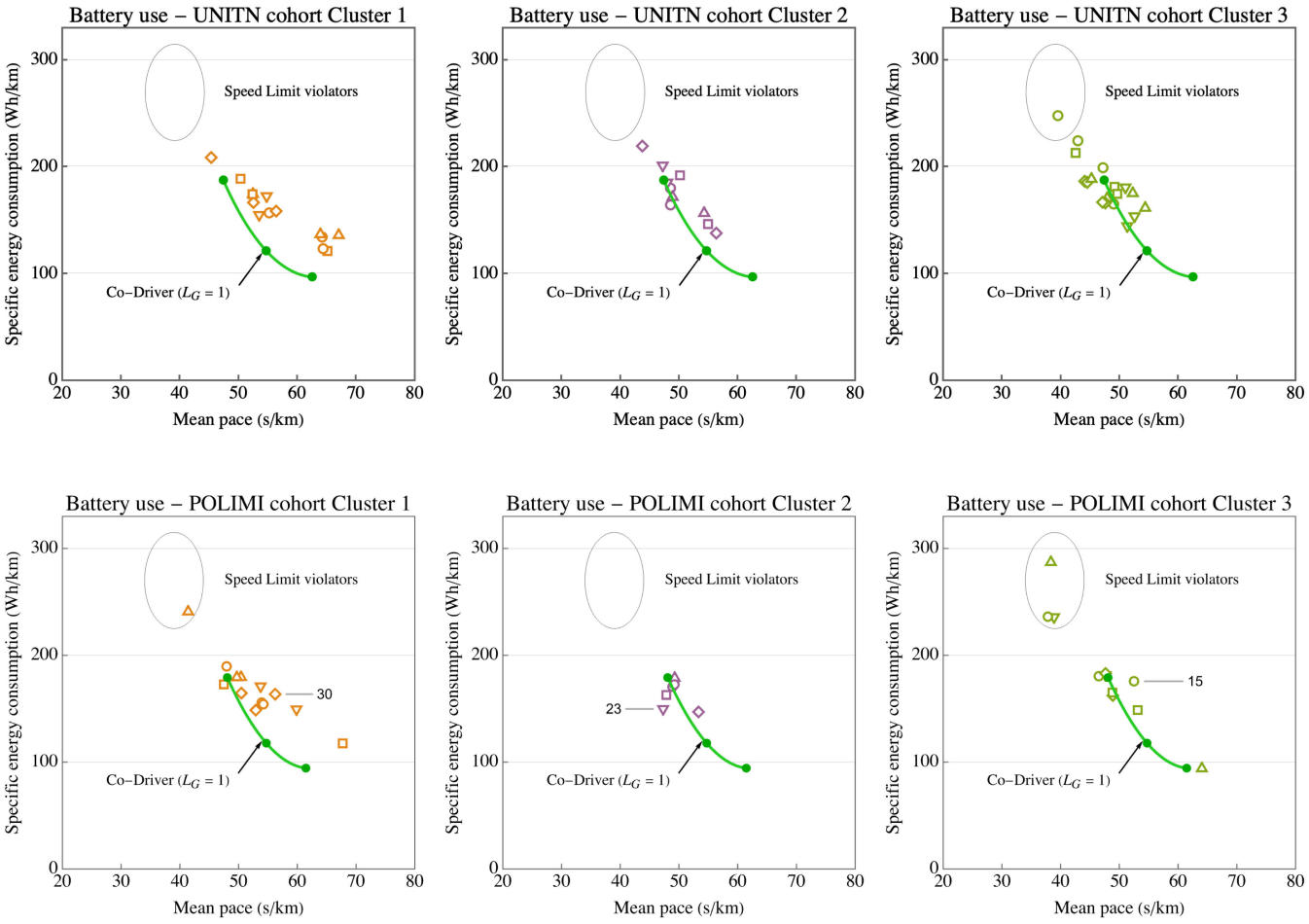

FIGURE 11. Specific energy consumption versus mean pace for the POLIMI testparticipants for the three participants' clusters.

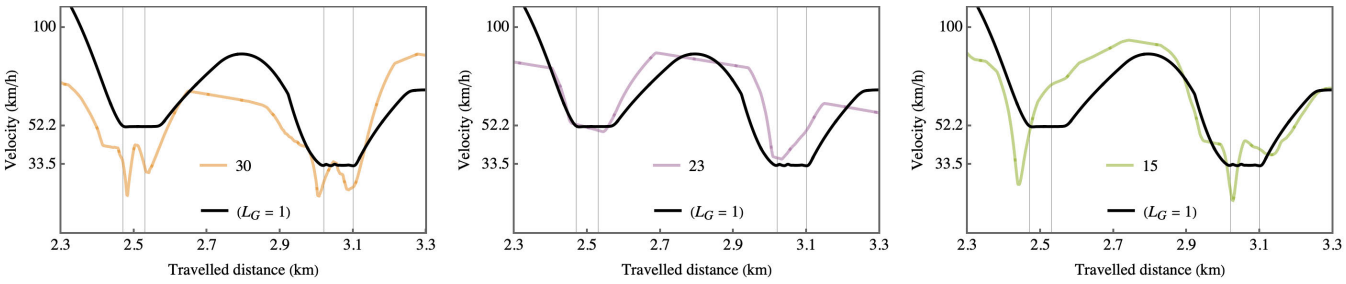

FIGURE 12. Speed of selected human drivers in the exit ramp and first roundabout.

with their more stable behavior observed in Figs. 8 and 9. Figure 13 illustrates the velocity profile of the top performer, participant 23. In the first curve (Fig. 12), he matches the speed of the co-driver but otherwise recovers speed earlier. He also employs a near-optimal driving style with prolonged coasting phases, which accounts for his relatively higher pace (Fig. 13). Finally, Cluster 3, which would be expected to lie to the left of the co-driver ($L_G = 1$) curve, includes three participants who are actually located on the right side. Figure 12 shows that one of them, participant 15, makes the same type of error as drivers in Cluster 1, but this occurs before reaching the curve.

Table 3 compares the energy losses of the three selected participants with those of the co-driver configured with $w = 10\%$[2] and $L_G = 1$. The most noticeable difference is the variability of the human drivers, who occasionally make mistakes that increase energy losses. The co-driver's

[2]A comparison with $w = 0$ would not reveal any substantial benefit, as the co-driver in that case closely mimics human braking before curves.

consistent, regular behavior is one reason to prefer it over human drivers, even though some humans, under constant attention, can be similarly efficient.

3) UNITN cohort

The analysis of the UNITN cohort largely confirmed the previous findings. The most notable difference was the absence of extreme speed violators, although a few mild violators were present. Another distinction was a slightly greater dispersion of the data points.

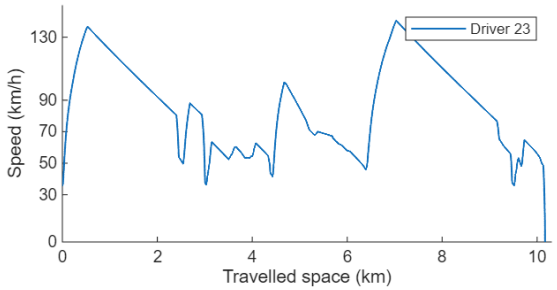

FIGURE 13. Speed profile of Driver 23. This driver achieved one of the highest average speeds at 76.1 km/h, with relatively low energy consumption of 150.7 km/h. The driving strategy was to accelerate to the legal speed limit (or just above), then immediately coast down and apply a mild brake before entering curves and roundabouts.

TABLE 3. Average speed and specific energy usage for a subset of drivers.

driver	speed (km/h)	total (W/km)	tires (W/km)	powertrain (W/km)	drag (W/km)	braking (W/km)
Co-Driver	65.8	120.4	40.9	19.4	49.3	10.8
15	68.6	175.2	40.9	30.4	72.3	31.5
23	76.1	150.7	40.9	24.6	74.8	10.3
30	64.0	164.7	40.9	29.5	65.9	28.5

C. SUBJECTIVE TEST RESULTS

In the previous section, drivers were compared with a co-driver set to $L_G = 1$, representing a median driver [35], [36]. During initial tests, however, we found that setting $L_G = 0.8$ provided a better experience, with fewer tendencies toward motion sickness. Another reason for lowering L_G was that the co-driver remained within its lane in roundabouts (Fig. 7), unlike human drivers, who often cross lanes and expect the co-driver to do the same. The reduced curve speed associated with $L_G = 0.8$ helped to mitigate this mismatch.

Based on these considerations, we conducted the subjective user tests with $L_G = 0.8$. This choice does not affect the quantitative comparisons from the previous chapter, but only the subjective opinions reported here. Hence, when evaluating the subjective results, it must be taken into account that drivers experienced three different situations at $L_G = 0.8$, marked by the labeled round dots in Fig. 10 and Fig. 11. This aspect will be taken into account in the discussion of the subjective findings.

In the following subsections, we present the statistical results of the subjective analysis.

The statistical methods are adapted to the type and structure of the reported outcomes: trial-related questionnaire items are analyzed using linear mixed-effects models to account for the repeated-measures structure of the data, whereas session-level questionnaire items are analyzed using between-subjects models, consistent with their single-observation-per-participant structure.

For all between-subjects ANOVA models reported in this section, variance homogeneity was assessed using median-centered Levene (Brown–Forsythe) tests, and residual normality was evaluated where applicable. When substantial deviations from normality were detected, nonparametric robustness checks were conducted to confirm the stability of the conclusions.

To ensure transparency and reproducibility, the complete statistical analysis supporting these results is documented in dedicated supplementary materials. The supplementary package includes the datasets used for the analysis, a fully documented analysis notebook that reproduces the reported statistical tests, effect sizes, assumption checks, and sensitivity analyses, and a self-contained, concise statistical summary.

The results presented in this section, therefore, focus on interpretation, while detailed statistical outputs are provided in the supplementary materials.

1) RELATION BETWEEN SIMULATOR, AGE, GENDER, AND PACE

Figure 14 illustrates the average driving pace in manual mode as a function of age, separated by gender and simulator. Manual-driving pace is measured once per participant and is therefore analyzed using between-subjects models. An analysis including the main effects of simulator, gender, and age group (18–25, 26–35, 36–45, 46–55, and 56–65 years) reveals no significant effects of simulator or age on pacing. Because age–gender cells in the UNITN cohort are sparsely populated, inference on demographic effects is based on the balanced POLIMI cohort. In this cohort, gender has a statistically significant effect on manual-driving pace, with female participants driving on average approximately 5.5 s/km slower than male participants ($p \approx 0.02$). The magnitude of this gender effect is large (partial $\eta_p^2 \approx 0.20$; Cohen's $d \approx 0.92$). Overall, these results indicate that, under manual-driving conditions, pacing differences are associated with gender rather than age, and that no systematic simulator-related effect on manual-driving pace is observed.

2) RELATION BETWEEN SIMULATOR, AGE, GENDER, AND ENERGY CONSUMPTION

Figure 15 shows the average energy consumption in manual driving mode as a function of age, separated by gender and simulator. Manual-driving energy consumption is analyzed analogously to driving pace using between-subjects models and shows no statistically significant effects of the simulator or age. As with manual-driving pace, inference on demographic effects is based on the balanced POLIMI cohort.

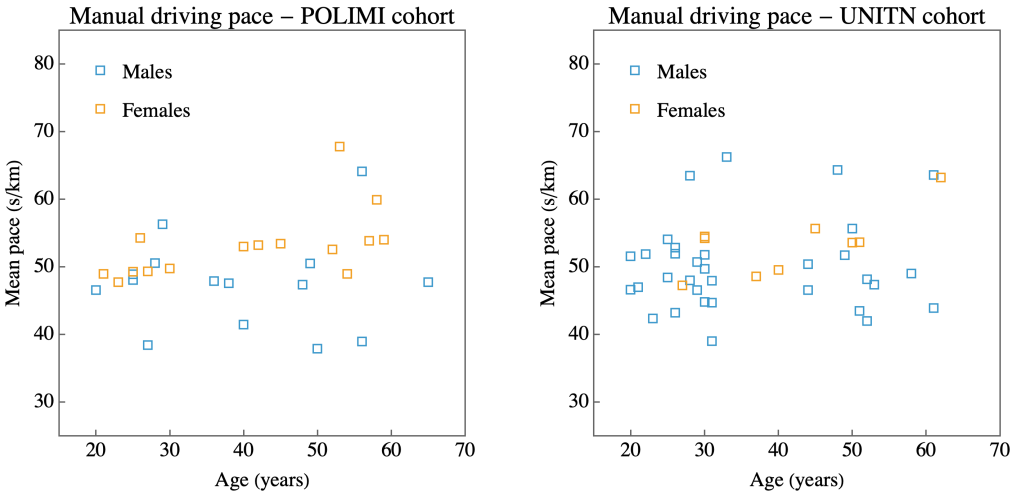

FIGURE 14. Manual-driving pace plotted as a function of age, separated by gender and simulator. Points represent individual participant measurements. Statistical inference on demographic effects is based on the balanced POLIMI cohort, as age–gender cells in the UNITN cohort are sparsely populated. In the POLIMI simulator, female participants drive on average 5.5 s/km slower than male participants ($p = 0.02$; partial $\eta_p^2 \approx 0.20$, Cohen's $d \approx 0.92$), while no significant effects of age or simulator on manual-driving pace are observed.

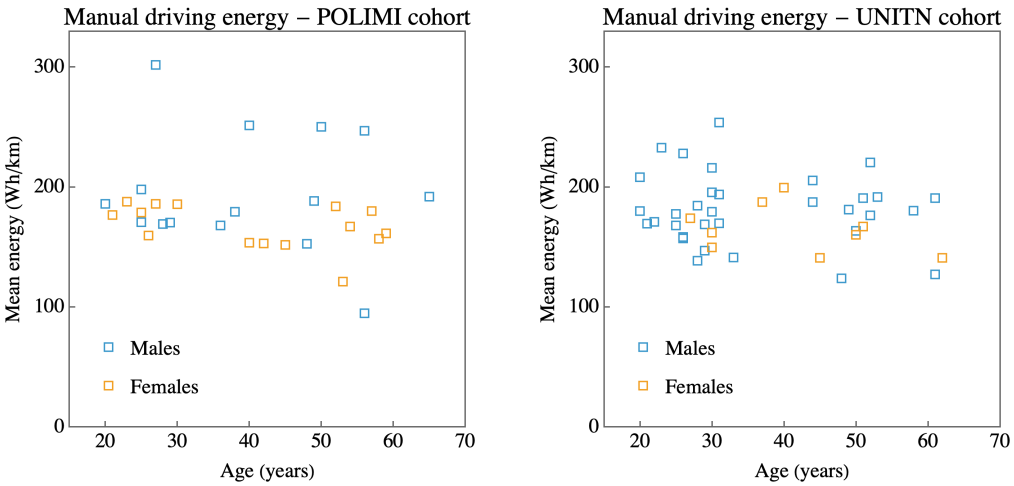

FIGURE 15. Manual-driving energy consumption plotted as a function of age, separated by gender and simulator. Points represent individual participant measurements. Statistical analyses indicate no systematic effects of age, gender, or simulator on manual-driving energy consumption.

In this cohort, neither age nor gender shows a statistically significant effect on energy consumption. However, a weak, non-robust gender trend is observed, with higher average consumption among male participants. Effect-size estimates for age and gender are small. Overall, these results indicate that, under manual driving conditions, energy consumption does not exhibit systematic differences associated with age, gender, or simulator.

3) TEST EXECUTION AND INTERVIEWS

As anticipated in Section III-A, the test procedure consisted of one session comprising four driving trials:

1) experience the non-green co-driver ($w = 0$),
2) experience the green co-driver at $w = 10\%$,
3) experience the green co-driver at $w = 50\%$,
4) drive the vehicle freely.

Trials 1, 2, and 3 were randomized, whereas Trial 4 was always administered last.

After Trials 1, 2, and 3, the drivers were shown the vehicle's autonomy and travel time, e.g., for UNITN[3]:

- 243 km and 9' 31'' for $w = 0\%$,
- 382 km and 10' 48'' for $w = 10\%$,
- 490 km and 12' 23'' for $w = 50\%$.

The corresponding pace and specific energy consumption are shown by the labeled green dots in Fig. 10.

[3]Similar figures hold for POLIMI.

Following Trial 4, we collected the manual-driving log, recording the speed and acceleration profiles, and computed each participant's pace and specific energy consumption. These values are shown by the squares in Fig. 10 and were also presented to the test drivers.

The following questions were asked at the end of each trial:

Q1 How do you rate the driving experience? - 1. Extremely boring ... 6. Very exciting.
Q2 How do you rate the driving situation? - 1. Extremely safe ... 6. Extremely risky.
Q2b Can you identify a risky situation?

At the end of the session (four trials), after recalling the autonomy and arrival times in the four trials, we asked the following final questions:

Q3 How do you rate the realism of the simulation? 1. Completely unrealistic ... 6. Completely realistic.
Q4 How do you rate the immersive nature of the experience? 1. Not at all engaging ... 6. Extremely engaging.
Q5 Would you be inclined to use an automatic eco-driving feature? 1. Never ... 6. Every day.
Q6 Which autonomous driving would you prefer? $w = 0$, $w = 10\%$ or $w = 50\%$?

Below, we present the answers organized by question.

Q1. Figure 16 illustrates the distribution of responses to Question 1 for the POLIMI and UNITN cohorts across the four driving modes {Manual driving, 0%, 10%, 50%}. As shown by the corresponding mean values in Fig. 17, the average score decreases monotonically when moving from manual driving to increasingly eco-oriented automated modes, with the lowest ratings observed for the slowest configuration ($w = 50\%$). The relative ordering of the four driving modes is qualitatively consistent across the two simulators. Trial-related Q1 responses were analyzed using linear mixed-effects models to account for the repeated-measures structure of the data. The analysis reveals a highly significant effect of driving mode on Q1 scores ($p < 0.001$), with a large associated effect size (partial $\eta_p^2 \approx 0.63$). A statistically significant but smaller simulator effect is also observed ($p = 0.016$, partial $\eta_p^2 \approx 0.025$), indicating modest simulator-dependent differences. Overall, these results show that the selected driving mode primarily drives perceived driving experience, while simulator-related effects are secondary. Detailed statistical results and robustness analyses are reported in the supplementary materials.

Q2. Figure 18 illustrates the distribution of responses to Question 2 (perceived risk) across the four driving modes. As shown by the corresponding mean values in Fig. 19, average risk ratings are almost constant across driving modes in the POLIMI simulator, and vary appreciably only in the UNITN simulator, where faster modes (Manual, $w = 0\%$) differ from slower ones ($w = 10\%, w = 50\%$). This pattern indicates a more moderate overall sensitivity of perceived risk to changes in driving mode compared with driving experience (Q1). Trial-related Q2 responses were analyzed using linear mixed-effects models to account for the repeated-measures structure of the data. The analysis revealed a statistically significant Driving Mode × Simulator interaction ($p < 0.001$), indicating that the effect of driving mode on perceived risk differed between simulators. Consequently, main effects were not interpreted directly, and follow-up mixed-effects models were fitted separately within each simulator. In the POLIMI simulator, Driving Mode did not significantly affect perceived risk ($p \approx 0.33$). In contrast, in the UNITN simulator, Driving Mode had a statistically significant effect ($p < 0.001$), with a large effect size (partial $\eta_p^2 \approx 0.31$). Post hoc comparisons indicated that perceived risk differed significantly between faster modes (Manual, $w = 0\%$) and slower modes ($w = 10\%$ and $w = 50\%$), consistent with Fig. 19. This simulator-specific effect may be explained by the less precise longitudinal control of the UNITN simulator, which produced jerkier behavior and a greater sense of insecurity at faster paces. Additional qualitative feedback collected through Question Q2b helps contextualize these results. Participants most frequently reported unfamiliar or uncomfortable behavior at roundabouts, particularly regarding speed selection and trajectory execution, with more complaints for UNITN. Feedback also mentioned unexpected braking or acceleration maneuvers and, in some cases, discomfort during highway exits at low speeds. Detailed statistical results and robustness analyses are reported in the supplementary materials.

Q3. Figure 20 illustrates the distribution of responses to Question 3 (realism of the simulation) for the POLIMI and UNITN cohorts. The average realism score is comparable across simulators and falls within slightly realistic evaluations, with the POLIMI simulator showing a slightly higher mean (4.07) than the UNITN simulator (3.76). Session-level Q3 responses (defined once per participant) were analyzed using between-subject models. Statistical analysis reveals that the observed difference in average realism ratings between simulators is not statistically significant ($p = 0.09$). No significant effects of age or gender are observed. Overall, the results indicate that perceived realism of the driving experience is similar across the two simulators, and that the small difference in average ratings does not reflect a systematic or statistically meaningful effect.

Q4. Figure 21 shows the distribution of responses to Question 4 (perceived immersion) for the POLIMI and UNITN simulators. In both simulators, the most frequent rating is very engaging, indicating a generally high level of perceived immersion. Session-level Q4 responses (defined once per participant) were analyzed using between-subject models. Simulator effects were assessed using the combined POLIMI and UNITN dataset. In contrast, age and gender effects were evaluated on the balanced POLIMI dataset, as age–gender cells in the UNITN cohort are sparsely populated. Statistical analysis reveals a significant effect of age on perceived immersion ($p \approx 0.045$), while no statistically significant effects of simulator or gender are observed. The magnitude of the age effect is substantial

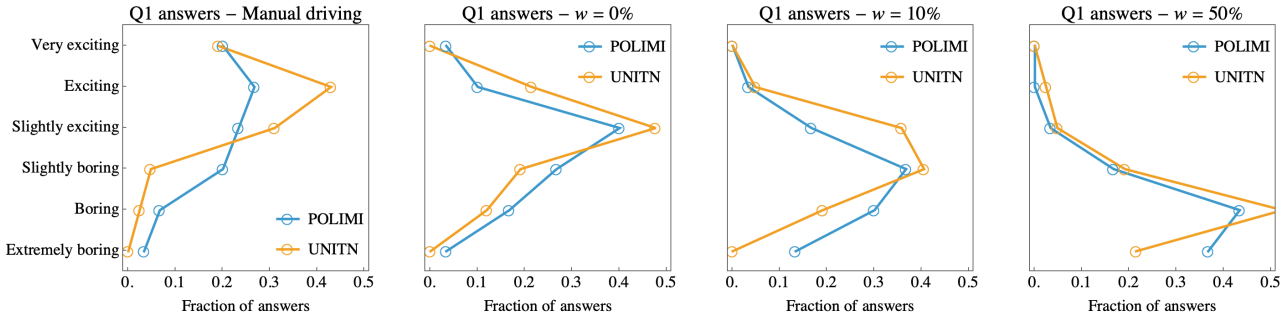

FIGURE 16. Distributions of responses to Question 1 (driving experience) across the four driving modes. The score decreases monotonically from manual driving to increasingly eco-oriented automated modes, with the lowest ratings observed for the slowest configuration ($w = 50\%$). Trial-related responses were analyzed using linear mixed-effects models accounting for the repeated-measures structure of the data. The analysis reveals a highly significant effect of driving mode ($p < 0.001$, partial $\eta_p^2 \approx 0.63$) and a smaller but statistically significant simulator effect ($p = 0.016$, partial $\eta_p^2 \approx 0.025$).

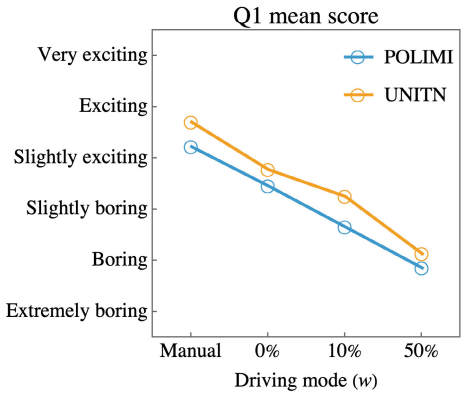

FIGURE 17. Mean response to Question 1 (driving experience) across the four driving modes. The average score decreases monotonically from manual driving to increasingly eco-oriented automated modes, with the lowest values observed for the slowest configuration ($w = 50\%$).

(partial $\eta_p^2 \approx 0.37$) and remains robust under the verified ANOVA assumptions. Overall, these results indicate that perceived immersion is primarily influenced by participant age rather than by simulator-specific characteristics.

Q5. Figure 22 illustrates the distribution of responses to Question 5 (propensity to use the system) for the POLIMI and UNITN cohorts. Overall, responses indicate a generally positive attitude toward system usage across participants. Session-level Q5 responses (defined once per participant) were analyzed using between-subject models. Because age–gender cells in the UNITN cohort are sparsely populated, inference on age and gender effects is based on the balanced POLIMI dataset. In this cohort, no statistically significant effects of age or gender on propensity-to-use scores are observed. Simulator effects were assessed using the combined POLIMI and UNITN dataset. Statistical analysis reveals a significant simulator effect, with higher average propensity-to-use scores in the UNITN simulator than in the POLIMI simulator ($p \approx 0.03$). The associated effect size is small to moderate (partial $\eta_p^2 \approx 0.09$, Cohen's $d \approx 0.51$). This result remains consistent when age and gender are included as covariates in the factorial model. Overall, these results indicate that participants' propensity to use the system is not systematically influenced by age or gender, while modest simulator-dependent differences are observed.

Q6. Fig. 23 shows that the preferred driving mode is between $w = 0\%$ and $w = 10\%$. Statistical analysis does not reveal significant effects of age, gender, or simulator on preferred trade-off selection.

4) RELATION BETWEEN PACE, SIMULATOR, AND Q1 SCORE

We hypothesized that the score for Question 1 might be associated with travel speed. Specifically, we examined the difference $\Delta Q1$ in Q1 scores between manual and green driving across the three modalities and compared it with the corresponding difference in pace. Figure 24 plots $\Delta Q1$ (manual minus green Q1 score) against the difference in pace (manual minus green pace) for both simulators and all three modalities. The effect of the simulator was not statistically significant, whereas the effect of the pace difference was ($p < 0.001$). The black line indicates a linear model fit, $\Delta Q1 = 0.80 - 0.086\Delta\text{pace}$ ($R^2 = 0.34$). This implies that, to achieve a similar Q1 score, green driving should be roughly 9 s/km faster than manual driving. The figure also uses colors to illustrate the regions associated with each of the three modalities.

IV. DISCUSSION

The results in this study should be interpreted in light of the simulator-based experimental setup. While driving simulators enable controlled and repeatable evaluations, they cannot fully capture all aspects of real-world driving. The findings, therefore, primarily indicate relative trends and behavioral effects, and on-road validation remains a necessary next step for deployment-oriented assessment.

Using two simulators with different fidelity levels reveals platform-dependent effects. At the same time, the consistency of qualitative trends across both platforms supports interpreting the results at the level of system behavior, while avoiding claims of simulator-independent quantitative performance.

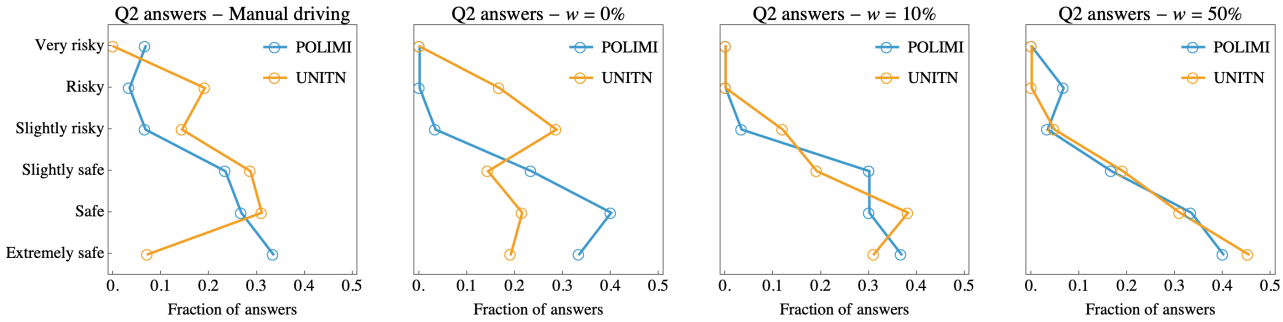

FIGURE 18. Distribution of responses to Question 2 (perceived risk) across the four driving modes, separated by simulator. Lines connect the percentage of responses associated with each Q2 rating. The distributions show limited variation in perceived risk across driving modes, with simulator-dependent differences.

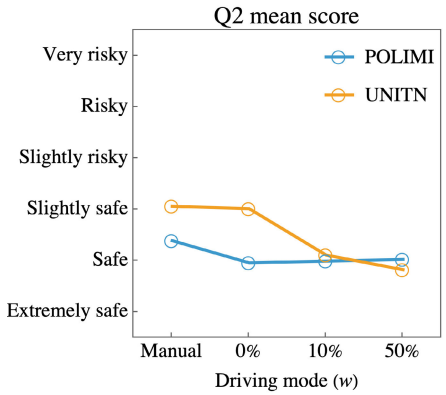

FIGURE 19. Mean response to Question 2 (perceived risk) across the four driving modes, separated by simulator. Average ratings show limited variation across driving modes, with simulator-dependent differences.

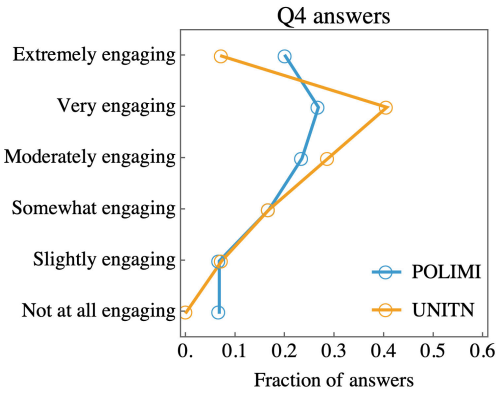

FIGURE 21. Distributions of responses to Question 4 (perceived immersion) for the POLIMI and UNITN simulators. In both simulators, the most frequent rating is very engaging. Statistical analysis reveals no significant effect of the simulator on perceived immersion, while age has a significant influence ($p \approx 0.045$, $\eta_p^2 \approx 0.37$) when assessed on the balanced POLIMI dataset.

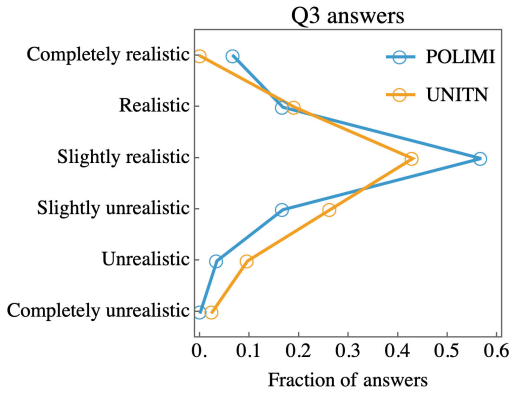

FIGURE 20. Distributions of responses to Question 3 (realism of the simulation) for the POLIMI and UNITN simulators. Ratings cluster around slightly realistic evaluations. The difference in average realism scores between simulators is not statistically significant ($p = 0.09$).

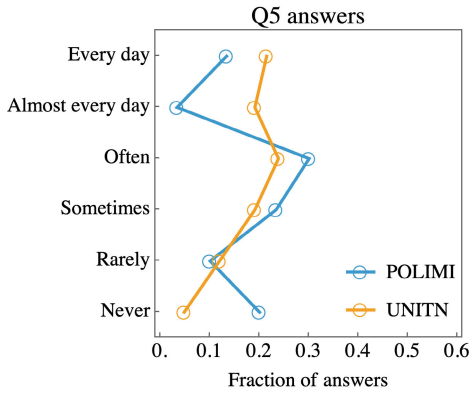

FIGURE 22. Distributions of responses to Question 5 (propensity to use an automatic eco-driving feature) for the POLIMI and UNITN simulators. Ratings indicate a generally positive inclination toward system use. A statistically significant simulator effect is observed, with higher average propensity-to-use scores in the UNITN simulator compared to the POLIMI simulator ($p \approx 0.03$; partial $\eta_p^2 \approx 0.09$, Cohen's $d \approx 0.51$).

We first consider the cost–benefit trade-off of different green-driving settings. At $w = 0\%$ (naturalistic driving), travel time is 9 minutes 31 seconds, and range is 243 km ($L_G = 0.8$ for UNITN). At $w = 10\%$, travel time increases to 10 minutes 48 seconds (+13.5%), but autonomy rises to 382 km (+57%). Thus, a small reduction in pace yields a large gain in energy savings and range, which is especially relevant for electric vehicles. For higher w, the benefits show diminishing returns (Fig. 10). As Fig. 5 illustrates, green-driving policies first reduce energy wasted in braking; further gains then require noticeably lower speeds and reduced

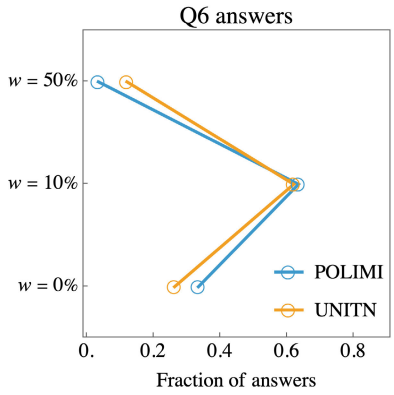

FIGURE 23. Distributions of responses to Question 6 (preferred autonomous driving trade-off). Most participants prefer mild eco-driving configurations, with the highest proportion selecting $w = 10\%$ and a smaller proportion selecting $w = 0\%$. Statistical analysis does not reveal significant effects of age, gender, or simulator on preferred trade-off selection.

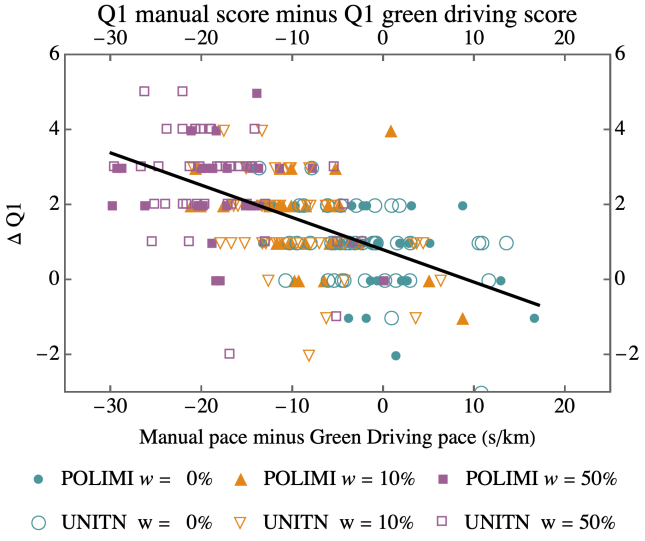

FIGURE 24. The extra score given to Q1 in manual driving depends on the difference in manual pace versus green driving pace.

aerodynamic drag. Participants preferred w values between 0% and 10% (Fig. 23), even though Q1 responses indicate that manual driving or $w = 0\%$ are perceived as more exciting (see Fig. 16 and Fig. 17). This suggests that many are willing to trade a slight loss in speed for a substantial increase in battery range.

In the driving simulators, Section III-C, the participants experienced $L_G = 0.8$ to limit motion sickness. In real cars, using $L_G = 1$ could make paces several seconds faster (Fig. 10); we speculate, as suggested in Section III-C4, that this might further strengthen the preference for energy-saving policies in the cost–benefit trade-off.

Another consideration involves naturalistic driving. Figs. 10 and 11 show that drivers cluster near the tip of the $L_G = 1$ curve, so the naturalistic-driving model ($w = 0\%$) reflects median driver behavior. Some drivers lie to the right of the curve, indicating less efficient driving due to imperfect or inconsistent speed control (see Fig. 12). Although we expect better speed regulation in real vehicles, the green-driving function can help drivers maintain an optimal policy and save energy. Other drivers fall to the left of the curve because they change lanes in roundabouts, and some (such as driver 23 in Fig. 13) appear to know how to execute near-optimal coasting phases.

One aspect that human participants disliked was the self-driving agent's behavior at roundabouts, where it stayed in its lane rather than changing lanes (Q2 and Q2b). However, in real driving situations, limited visibility and traffic often cause both the human driver and the system to yield at the roundabout entrance, minimizing this difference. In any case, the green-driving function could be implemented as a standalone, longitudinal-only Advanced Driving Assistance System (ADAS)—letting humans handle lane changes—for example, integrated with an Adaptive Cruise Control (ACC) system, without requiring a separate self-driving agent.

V. CONCLUSION

The two simulator-based experiments in this study indicated that the Green Co-Driver can potentially improve the energy efficiency of electric vehicles while balancing naturalistic driving expectations.

Compared to human drivers under the tested simulator conditions, the co-driver exhibited more regular longitudinal behavior and lower dispersion in energy consumption. Human drivers were, generally, less efficient and regular.

Efficiency gains arose mainly from extended coasting phases, which reduced mechanical and regenerative braking losses. Moderate green-driving bias levels ($w = 10\%$) provided substantial energy savings with only a minor increase in travel time, indicating that much of the potential efficiency benefit can be captured without noticeably degrading trip duration.

System success depends on both efficiency and driver acceptance. Participants expressed willingness to use the system when moderate settings ($w = 10\%$) offered a good balance between energy savings and comfort.

The Green Co-Driver appears flexible, regular, and repeatable under the simulated conditions. Besides enhancing EV efficiency, it can also help promote eco-driving awareness.

Differences between the UNITN and POLIMI simulators influenced subjective perception; however, overall trends remained consistent across platforms.

Future work should explore more complex traffic scenarios and on-road vehicle testing to better balance energy efficiency with user acceptance beyond the simulator-based proof-of-concept presented in this paper. These considerations support interpreting the results at the level of system behavior, while avoiding claims of direct real-world deployment beyond the simulator-based proof-of-concept presented here.

FIGURE 25. The driving Simulator of the University of Trento uses a 3 degrees of freedom platform that reproduces heave, pitch, and roll motion in an immersive wide screen.

FIGURE 26. POLIMI 9-dof cable-driven dynamic driving simulator moving over the 6 × 6-meter platform.

APPENDIX: THE DRIVING SIMULATORS

For this research, two driving simulators have been utilized. One is the high-fidelity cable-driven simulator at the DRISMI lab, Politecnico di Milano, and the other is the 3-DOF semi-static simulator at the Simulation and Virtual Reality Lab at the University of Trento.

A. SEMI-STATIC DRIVING SIMULATOR (UNITN)

The semi-static simulator is a 3 DOF platform that captures the heave, pitch, and roll motion of a car. The setup at UNITN (Fig. 25) features a 210°-wide projector screen in front of a motion platform that uses four linear actuators to achieve 100 mm of heave, 7.9° of roll, and 5.1° of pitch. It can also produce vibrations up to 100 Hz for noise, vibration, and harshness emulation. The platform is supported by software packages, which manage motion cueing algorithms and kinematic inversion.

The cockpit system features gas, brake, and clutch pedals, along with a steering system.

The virtual simulation tool used was CarMaker 11.0 [43]. CarMaker integrates with the simulator hardware via an asynchronous ZMQ communication architecture [44], operating at 1000 Hz. The IPG Movie component of Carmaker allows for graphical visualization of simulations.

The wide-screen projector displays IPG Movie visuals for the driver on the motion platform. The worst-case latency between user input and motion platform response is estimated at 12 ms to 15 ms, which helps mitigate motion sickness [45]. The actuation latency of the linear actuators is 8 ms.

B. HI-FIDELITY DRIVING SIMULATOR (PoliMI)

POLIMI operates a mid-size dynamic driving simulator which is actuated by a cable-driven system, as shown in Figure 26. The cable actuation enables wide-range displacements; for instance, a lane-change maneuver can be reproduced at full 1:1 scale. The system moves a disk frame, supported by air pads, across a 6 × 6 meter platform. Cables control the disk frame's horizontal translations and yaw motion, with a bandwidth of approximately 3 Hz. A hexapod mounted on top of the disk frame adds six additional degrees of freedom, controlling the heave, roll, and pitch of the cockpit of a compact car. With a bandwidth of up to 30 Hz, the hexapod also introduces high-frequency components into the motion, including horizontal-plane translations and yaw. Eight shakers (bandwidth: 200 Hz) are installed in the cockpit to reproduce vibrations from road irregularities and the powertrain.

To enhance driver perception, the seat is equipped with pneumatic cushions that inflate during acceleration or cornering to simulate sustained forces. Pneumatically controlled seat belts further enhance realism by tightening during braking. Active steering and braking systems provide force feedback directly on the steering wheel and brake pedal. Immersion and realism are further enhanced through advanced graphics, with detailed driving scenarios projected onto a 270° screen that surrounds the driver. Table 4 collects the main features of DIM 400.

The simulator is powered by a 14-degree-of-freedom (14 DOF) vehicle model developed within VI-CarRealTime. environment [46].

The platform's motion is managed through a cueing algorithm based on a Model Predictive Control (MPC) framework. At each time step t_k, the vehicle model calculates the accelerations and angular velocities of the cockpit in the ''virtual'' car. These signals are then processed as follows:

- Scaling – since the hardware can only reproduce them within certain limits (Table 4).
- Low-pass filtering – applied to lateral and longitudinal accelerations to generate inputs for tilt coordination, where the cockpit tilts to replicate the low-frequency components of motion.
- High-pass filtering – used to extract the high-frequency dynamics.

TABLE 4. Main features of POLIMI driving simulator.

Physical quantity	Values
Platform size	6m x 6m
Latency	25 ms
Lateral travel	4.2 m
Vertical travel	± 298 mm
Max Longitudinal acceleration	1.5 g
Max Lateral acceleration	1.5 g
Max Vertical acceleration	2.5 g
Longitudinal travel	4.2 m
Yaw angle	± 62°
Roll angle	± 15°
Pitch angle	± 15°
Visual system	270°

- Vestibular filtering – all signals are passed through transfer functions modeling the human vestibular system's response [47].

The result of this processing is a reference vector r_k, representing the accelerations and angular velocities that the driver should perceive. The MPC controller computes the input vector u_k needed to achieve this target. In parallel, a real-time multi-body model of the moving platform estimates the actual accelerations and angular velocities y_k perceived by the driver's vestibular system in the simulator. The controller then determines u_k by minimizing the difference between r_k and y_k. Additionally, the MPC framework enforces displacement constraints to ensure the disk frame remains within the available workspace.

ACKNOWLEDGMENT

The authors gratefully acknowledge Antonio Cioffi for his former contributions to the research and Prof. Paolo Bosetti for valuable comments and discussions on the statistical analysis. Views and opinions expressed are, however, those of the authors only and do not necessarily reflect those of the European Union or European Commission. Neither the European Union nor the granting authority can be held responsible for them.

USE OF AI (GRAMMARLY AND OpenAI)

The authors used Grammarly (https://www.grammarly.com) for language and grammar enhancement. ChatGPT was used solely to assist with text restructuring. All content was reviewed and finalized by them.

REFERENCES

[1] F. Chen, N. Taylor, and N. Kringos, "Electrification of roads: Opportunities and challenges," *Appl. Energy*, vol. 150, pp. 109–119, Jul. 2015.

[2] A. E. af Wåhlberg, "Long-term effects of training in economical driving: Fuel consumption, accidents, driver acceleration behavior and technical feedback," *Int. J. Ind. Ergonom.*, vol. 37, no. 4, pp. 333–343, Apr. 2007.

[3] Y. Huang, E. C. Y. Ng, J. L. Zhou, N. C. Surawski, E. F. C. Chan, and G. Hong, "Eco-driving technology for sustainable road transport: A review," *Renew. Sustain. Energy Rev.*, vol. 93, pp. 596–609, Oct. 2018.

[4] W. Ke, S. Zhang, X. He, Y. Wu, and J. Hao, "Well-to-wheels energy consumption and emissions of electric vehicles: Mid-term implications from real-world features and air pollution control progress," *Appl. Energy*, vol. 188, pp. 367–377, Feb. 2017.

[5] A. Castaings, W. Lhomme, R. Trigui, and A. Bouscayrol, "Comparison of energy management strategies of a battery/supercapacitors system for electric vehicle under real-time constraints," *Appl. Energy*, vol. 163, pp. 190–200, Feb. 2016.

[6] W. Shabbir and S. A. Evangelou, "Threshold-changing control strategy for series hybrid electric vehicles," *Appl. Energy*, vol. 235, pp. 761–775, Feb. 2019.

[7] Z. Wei, J. Xu, and D. Halim, "HEV power management control strategy for urban driving," *Appl. Energy*, vol. 194, pp. 705–714, May 2017.

[8] F. Ding, X. Luo, G. Li, H. H. Tew, J. Y. Loo, C. W. Tong, A. S. M. Bakibillah, Z. Zhao, and Z. Tao, "Energy-efficient hybrid model predictive trajectory planning for autonomous electric vehicles," in *Proc. IEEE Int. Conf. Syst., Man, Cybern. (SMC)*, Oct. 2024, pp. 1263–1269.

[9] A. Sciarretta, G. De Nunzio, and L. L. Ojeda, "Optimal ecodriving control: Energy-efficient driving of road vehicles as an optimal control problem," *IEEE Control Syst. Mag.*, vol. 35, no. 5, pp. 71–90, Oct. 2015.

[10] D. L. Schall and A. Mohnen, "Incentivizing energy-efficient behavior at work: An empirical investigation using a natural field experiment on eco-driving," *Appl. Energy*, vol. 185, pp. 1757–1768, Jan. 2017.

[11] Y. Xu, H. Li, H. Liu, M. O. Rodgers, and R. L. Guensler, "Eco-driving for transit: An effective strategy to conserve fuel and emissions," *Appl. Energy*, vol. 194, pp. 784–797, May 2017.

[12] D. Maamria, K. Gillet, G. Colin, Y. Chamaillard, and C. Nouillant, "Computation of eco-driving cycles for hybrid electric vehicles: Comparative analysis," *Control Eng. Pract.*, vol. 71, pp. 44–52, Feb. 2018.

[13] D. Shen, D. Karbowski, and A. Rousseau, "A minimum principle-based algorithm for energy-efficient eco-driving of electric vehicles in various traffic and road conditions," *IEEE Trans. Intell. Vehicles*, vol. 5, no. 4, pp. 725–737, Dec. 2020.

[14] X. Yan, C. K. Allison, J. M. Fleming, N. A. Stanton, and R. Lot, "The benefit of assisted and unassisted eco-driving for electrified powertrains," *IEEE Trans. Human-Mach. Syst.*, vol. 51, no. 4, pp. 403–407, Aug. 2021.

[15] Y. Hu, C. Chen, J. He, and B. Yang, "Eco-platooning for cooperative automated vehicles under mixed traffic flow," *IEEE Trans. Intell. Transp. Syst.*, vol. 22, no. 4, pp. 2023–2034, Apr. 2021.

[16] Y. J. J. Heuts, R. Velpari, and M. C. F. Donkers, "Eco-driving and road curvature estimation: Retrospective analysis of experimental data of a fully electric coach," *Energy*, vol. 334, Oct. 2025, Art. no. 137526.

[17] T. Jayson, A. S. M. Bakibillah, C. P. Tan, M. A. S. Kamal, V. Monn, and J.-I. Imura, "Electric vehicle eco-driving strategy at signalized intersections based on optimal energy consumption," *J. Environ. Manage.*, vol. 368, Sep. 2024, Art. no. 122245.

[18] E. Mintsis, E. I. Vlahogianni, E. Mitsakis, and S. Ozkul, "Enhanced speed advice for connected vehicles in the proximity of signalized intersections," *Eur. Transp. Res. Rev.*, vol. 13, no. 1, pp. 1–14, Dec. 2021.

[19] A. S. M. Bakibillah, M. A. S. Kamal, C. P. Tan, T. Hayakawa, and J.-I. Imura, "Fuzzy-tuned model predictive control for dynamic eco-driving on hilly roads," *Appl. Soft Comput.*, vol. 99, Feb. 2021, Art. no. 106875.

[20] L. L. Ojeda, J. Han, A. Sciarretta, G. De Nunzio, and L. Thibault, "A real-time eco-driving strategy for automated electric vehicles," in *Proc. IEEE 56th Annu. Conf. Decis. Control (CDC)*, Dec. 2017, pp. 2768–2774.

[21] J. Han, A. Sciarretta, L. L. Ojeda, G. De Nunzio, and L. Thibault, "Safe- and eco-driving control for connected and automated electric vehicles using analytical state-constrained optimal solution," *IEEE Trans. Intell. Vehicles*, vol. 3, no. 2, pp. 163–172, Jun. 2018.

[22] Z. Su and P. Chen, "Eco-driving for battery electric vehicles using traffic-aware computationally efficient model predictive control," *IFAC-PapersOnLine*, vol. 55, no. 37, pp. 700–705, 2022.

[23] J. Xue, X. Jiao, D. Yu, and Y. Zhang, "Predictive hierarchical eco-driving control involving speed planning and energy management for connected plug-in hybrid electric vehicles," *Energy*, vol. 283, Nov. 2023, Art. no. 129058.

[24] Z. Yang, Z. Zheng, J. Kim, and H. Rakha, "Eco-driving strategies using reinforcement learning for mixed traffic in the vicinity of signalized intersections," *Transp. Res. C, Emerg. Technol.*, vol. 165, Aug. 2024, Art. no. 104683.

[25] D. Heyes, T. J. Daun, A. Zimmermann, and M. Lienkamp, "The virtual driving coach–design and preliminary testing of a predictive eco-driving assistance system for heavy-duty vehicles," *Eur. Transp. Res. Rev.*, vol. 7, no. 3, pp. 1–13, Sep. 2015.
[26] S. K. Chada, D. Görges, A. Ebert, R. Teutsch, and S. P. Subramanya, "Evaluation of the driving performance and user acceptance of a predictive eco-driving assistance system for electric vehicles," *Transp. Res. C, Emerg. Technol.*, vol. 153, Aug. 2023, Art. no. 104193.
[27] J. Guanetti, Y. Kim, and F. Borrelli, "Control of connected and automated vehicles: State of the art and future challenges," *Annu. Rev. Control*, vol. 45, pp. 18–40, 2018.
[28] M. Karrouchi, I. Nasri, M. Rhiat, I. Atmane, K. Hirech, A. Messaoudi, M. Melhaoui, and K. Kassmi, "Driving behavior assessment: A practical study and technique for detecting a driver's condition and driving style," *Transp. Eng.*, vol. 14, Dec. 2023, Art. no. 100217.
[29] J. Fleming, X. Yan, and R. Lot, "Incorporating driver preferences into eco-driving assistance systems using optimal control," *IEEE Trans. Intell. Transp. Syst.*, vol. 22, no. 5, pp. 2913–2922, May 2021.
[30] R. Lot, J. Fleming, B. Chen, and S. Evangelou, "Eco-driving optimal control for electric vehicles with driver preferences," *Transp. Eng.*, vol. 19, Mar. 2025, Art. no. 100302.
[31] M. Da Lio, R. Donà, G. P. R. Papini, and A. Plebe, "The biasing of action selection produces emergent human-robot interactions in autonomous driving," *IEEE Robot. Autom. Lett.*, vol. 7, no. 2, pp. 1254–1261, Apr. 2022.
[32] P. Cisek, "Cortical mechanisms of action selection: The affordance competition hypothesis," *Phil. Trans. Roy. Soc. B, Biol. Sci.*, vol. 362, no. 1485, pp. 1585–1599, Sep. 2007.
[33] A. N. Meltzoff, "The 'like me' framework for recognizing and becoming an intentional agent," *Acta Psychologica*, vol. 124, no. 1, pp. 26–43, Jan. 2007.
[34] D. E. Kirk, *Optimal Control Theory: An Introduction*. Mineola, NY, USA: Dover, 2012.
[35] P. Bosetti, M. Da Lio, and A. Saroldi, "On curve negotiation: From driver support to automation," *IEEE Trans. Intell. Transp. Syst.*, vol. 16, no. 4, pp. 2082–2093, Aug. 2015.
[36] P. Bosetti, M. Da Lio, and A. Saroldi, "On the human control of vehicles: An experimental study of acceleration," *Eur. Transp. Res. Rev.*, vol. 6, no. 2, pp. 157–170, Jun. 2014.
[37] M. Da Lio, A. Mazzalai, K. Gurney, and A. Saroldi, "Biologically guided driver modeling: The stop behavior of human car drivers," *IEEE Trans. Intell. Transp. Syst.*, vol. 19, no. 8, pp. 2454–2469, Aug. 2018.
[38] J. M. Fleming, X. Yan, and R. Lot, "Fitting cornering speed models with one-class support vector machines," in *Proc. IEEE Intell. Vehicles Symp. (IV)*, Jun. 2019, pp. 2457–2462.
[39] M. A. Patterson and A. V. Rao, "GPOPS-II: A MATLAB software for solving multiple-phase optimal control problems using hp-adaptive Gaussian quadrature collocation methods and sparse nonlinear programming," *ACM Trans. Math. Softw.*, vol. 41, no. 1, pp. 1–37, Oct. 2014.
[40] Dreams4Cars. (2020). *Dream-like Simulation Abilities for Automated Cars*. Accessed: Dec. 5, 2024. [Online]. Available: https://www.dreams4cars.eu
[41] M. D. Lio, R. Donà, G. P. R. Papini, and K. Gurney, "Agent architecture for adaptive behaviors in autonomous driving," *IEEE Access*, vol. 8, pp. 154906–154923, 2020.
[42] M. Da Lio, A. Cherubini, G. P. R. Papini, and A. Plebe, "Complex self-driving behaviors emerging from affordance competition in layered control architectures," *Cognit. Syst. Res.*, vol. 79, pp. 4–14, Jun. 2023.
[43] IPG Automotive. (2025). *Carmaker*. Accessed: Jul. 2, 2025. [Online]. Available: https://www.ipg-automotive.com/en/products-solutions/software/carmaker/
[44] P. Hintjens, *ZeroMQ: Messaging for Many Applications*. Sebastopol, CA, USA: O'Reilly Media, 2013.
[45] S. Melzi and G. Previati, "Driving simulator: Analysing the impact of mechanical latency on the perception of lateral dynamics," *J. Vibrat. Control*, vol. 31, nos. 7–8, pp. 1510–1523, Apr. 2025.
[46] VI-grade. (2025). *VI-CarRealTime*. Accessed: Aug. 22, 2025. [Online]. Available: https://www.vi-grade.com/en/products/vi-carrealtime/
[47] Y. R. Khusro, Y. Zheng, M. Grottoli, and B. Shyrokau, "MPC-based motion-cueing algorithm for a 6-DOF driving simulator with actuator constraints," *Vehicles*, vol. 2, no. 4, pp. 625–647, Dec. 2020.

MAURO DA LIO (Member, IEEE) is a Full Professor of mechanical systems with the University of Trento, Italy. His earlier research activity was modeling, simulation, and optimal control of mechanical multibody systems, particularly vehicle and spacecraft dynamics. His current focus shifted to modeling human sensory-motor control with applications in health, robotics, and, mostly, and intelligent vehicles. He was involved in several EU framework programs six and seven projects (PReVENT, SAFERIDER, interactIVe, VERITAS, AdaptIVe, No-Tremor, and SUNRISE). He was the Coordinator of the EU Horizon 2020 Dreams4Cars Research and Innovation Action: a collaborative project in the robotics domain that aimed at increasing the cognition abilities of artificial driving agents using offline simulation mechanisms broadly inspired by the human dream state (learning of forward models and offline synthesis of inverse ones).

VISHNUVARDHAN SHAKTHIBALA received the M.Sc. degree in space engineering from the Politecnico di Milano, Milan, Italy. He is currently pursuing the Ph.D. degree in spacecraft guidance, navigation, and control with the Department of Electrical and Energy Engineering, University of Rome "La Sapienza," Italy. He has industry experience with Stellantis and Electrolux, where he contributed to the rapid prototyping of advanced driver assistance systems (ADAS) and functional system validation. He was a Research Fellow with the University of Trento's Simulation and Virtual Reality Laboratory, Trento, Italy, where he contributed to the Green Co-Driver Project. His work focused on integrating autonomous driving functionalities using hardware-in-the-loop setups and simulation environments, such as CarMaker and CARLA.

ANTONELLO CHERUBINI received the degree in mechanical engineering from the Politecnico di Milano, Italy, in 2012, and the Ph.D. degree in robotics from the Sant'Anna University of Pisa, Italy, in 2017. He has been a Visiting Research Fellow with TU Delft, The Netherlands; and a Visiting Professor with the University Carlos III of Madrid, Getafe, Spain. From 2022 to 2025, he was an Assistant Professor (RTDA) with the University of Trento, Trento, Italy. In July 2025, he moved to the Smart and Sustainable Transport Unit, Joint Research Centre (JRC) of European Commission, as a Project Officer. Since November 2025, he has been an Assistant Professor (RTT) with the University of Bologna, Italy. His Ph.D. thesis won the Prize Bernardo Nobile.

GASTONE PIETRO ROSATI PAPINI (Member, IEEE) received the degree in automation engineering from the University of Pisa, in 2012, and the Ph.D. degree from the Sant'Anna School of Advanced Studies in Emerging Digital Technologies, in 2016. He is currently an Associate Professor in advanced control systems applied to the field of autonomous driving and ADAS with the Department of Industrial Engineering, University of Trento. He is also the Co-Founder of Cheros s.r.l., a spinout company from the University of Pisa, specializes in renewable energies and ICT solutions. With over five years of experience in mechanics and control systems, he has focused on the application of machine learning techniques for modeling and controlling mechanical systems. His webpage is: https://tonegas.com/

STEFANO MELZI (Member, IEEE) is a Full Professor of applied mechanics with the Politecnico di Milano. Over more than 20 years, he has gained extensive experience and developed expertise in the experimental characterization of ground vehicles and their components, modeling techniques for complex systems, innovative sensing devices (such as smart tires), signal processing, and real-time applications. In 2020, he joined a research group of six professors to establish DrSMi, the Driving Simulator of Politecnico di Milano. Since 2021, he has been using this facility to analyze the interaction between drivers and ADAS. His research focuses on the dynamics of mechanical systems, with particular emphasis on ground vehicles.

ALESSANDRO REGAZZETTI is a Mechanical Engineer with the Politecnico di Milano. He was a Research Fellow with the Politecnico di Milano, Driving Simulator, contributing to the Green Co-Driver Project and to research on dynamic simulations for safer road systems.

STEFANO LOVATO received the M.Sc. degree in mechanical engineering, in 2020, and the Ph.D. degree in industrial engineering, in 2024. He is a Junior Assistant Professor with the University of Padua. Since 2020, his research has been focuses on the modeling, dynamics, and control of two- and four-wheeled road vehicles, particularly stabilization systems for two-wheeled vehicles and optimal control.

ROBERTO LOT is currently a Professor of mechanics of machines with the University of Padua, Italy. From 2014 to 2019, he was a Professor of automotive engineering with the University of Southampton, U.K. He has 30 years of experience in the automotive sector, contributing to the safety, performance, and energy efficiency of road and race vehicles.